

Research Article

A New Improved Kurtogram and Its Application to Bearing Fault Diagnosis

Xinghui Zhang,¹ Jianshe Kang,¹ Lei Xiao,² Jianmin Zhao,¹ and Hongzhi Teng¹

¹Mechanical Engineering College, Shijiazhuang 050003, China

²The State Key Lab of Mechanical Transmission, Chongqing University, Chongqing 400030, China

Correspondence should be addressed to Xinghui Zhang; dynamicbnt@163.com

Received 11 January 2015; Revised 3 March 2015; Accepted 3 March 2015

Academic Editor: Tai Thai

Copyright © 2015 Xinghui Zhang et al. This is an open access article distributed under the Creative Commons Attribution License, which permits unrestricted use, distribution, and reproduction in any medium, provided the original work is properly cited.

A new improved Kurtogram was proposed in this paper. Instead of Kurtosis, correlated Kurtosis of envelope signal extracted from the wavelet packet node was used as an indicator to determine the optimal frequency band. Correlated Kurtosis helps to determine the fault related impulse signals not affected by other unrelated signal components. Finally, two simulated and three experimental bearing fault cases are used to validate the effectiveness of proposed method and to compare with other similar methods. The results demonstrate it can locate resonant frequency band with a high reliability than two previous developed methods by Lei et al. and Wang et al. especially for the incipient faults under low load.

1. Introduction

Costs caused by failure of key components are huge for most complex and expensive machineries. Taking drivetrains as an example, they are widely used in wind turbines, nuclear power plants, hydropower stations, airplanes, helicopters, and so forth. In these drivetrains, bearings are critical components. They usually operate under hostile environments with high stress. The cost of replacement of bad bearing on offshore wind turbine gearbox will be 8,000\$ and 60,000\$ in addition to renting a crane [1]. If a bearing of helicopter gearbox fails, it may lead to a catastrophic disaster. Those findings emphasize why bearing fault diagnosis is very important in order to prevent unplanned failure and maintenance cost.

Fault diagnosis of rotating machinery has half-century history. In recent 15 years, many fault diagnosis methods were developed based on machine learning methods [2–4]. These methods mainly rely on amount of fault samples to train the model becoming very useful for online automotive fault diagnosis. However, because of the complex operating conditions, the high rate of false alarm is a significant problem which affects their performance. Implementing only machine learning methods for fault diagnosis methods does

not give a desirable result. Operating conditions of rotating machinery are usually very hostile and it is not rare case with simultaneously multiple faults. Even more, for complex machinery, it is very difficult to collect enough fault samples in order to properly train the machine learning methods. This is also the reason why many researchers prefer using frequency spectrum analysis methods for fault diagnosis. These frequency analysis methods have universal property and need less fault samples.

Randall and Antoni [5] gave a detailed tutorial on rolling element bearing diagnosis and consider envelope analysis (high frequency resonance technique) as fundamental and effective method for bearing fault detection. However, first step is to find the frequency band that contains intense impulse signals produced by bearing faults, and on the other hand, frequency band selection directly affects the performance of envelope analysis. There are two major research directions during 21st century in bringing bearing fault frequencies more obvious.

The first one is to enhance the impulse signals produced by faults. Sawalhi et al. [6] used minimum entropy deconvolution (MED) technique to deconvolve the effect of

transmission path which can bring clear impulses. Then, spectral Kurtosis (SK) was used to determine the appropriate frequency band which can be used to do the envelope analysis. Barszcz and Sawalhi [7] used MED to enhance the fault diagnosis of bearing of wind turbine. In the paper, parameters selection problem of MED has been discussed. Afterwards, in order to overcome the deficiency of MED, McDonald et al. [8] developed a new deconvolution method named maximum correlated Kurtosis deconvolution (MCKD). Besides of these two deconvolution methods, Karimi [9] used blind deconvolution, an image processing method, to improve the signal-to-noise ratio (SNR) of bearing fault signal. Recently, Raj and Murali [10] used Lucy-Richardson deconvolution to enhance the bearing fault detection. In addition, there are many other methods for enhancing the impulse signals produced by faults. However, these methods also have their limitations. Fault signals of interest are not present independently. Usually there is presence of fault signals from other components with noise in addition. Take gearbox, for example, as complex machinery with multiple gears, shaft, and bearing as fault potential components. The vibrations of gear faults are stronger than bearing faults making it very difficult to detect the bearing fault.

The second one is to find the frequency band which contains the strongest impulse signals produced by bearing fault [11–14]. Since spectral Kurtosis has been defined by Antoni [15], it was investigated for the diagnosis of rotating machinery faults. Then, Antoni [16] proposed two methods to calculate spectral Kurtosis. It is based on short time Fourier transform (STFT) (called Kurtogram for finding the optimal filter) and the other is based on 1/3 binary filter banks (fast Kurtogram for online condition monitoring and fault diagnosis). Recently, Lei et al. [12] indicated that a STFT based or filters-based spectral Kurtosis was not as precise as wavelet packet decomposition (WPD). They used WPD to replace the STFT in extracting transient characteristics and measured the Kurtosis of the temporal signal filtered by WPD. Barszcz and Jabłoński [11] proposed a new frequency band determination method named protrogram which is based on the Kurtosis of the envelope spectrum of the demodulated signal rather than the Kurtosis of the filtered time signal. Wang et al. [13] developed an enhanced Kurtogram. In this case Kurtosis values were calculated based on the power spectrum of the envelope of the signals extracted from wavelet packet nodes at different depths. Instead of traditional Daubechies wavelets, Chen et al. [14] used dual tree complex wavelet transform to decompose the signal. And then, a new enhanced signal impulsiveness evaluating indicator, named “spatial-spectral ensemble Kurtosis,” was used to determine the optimal frequency band which will be used for the envelope analysis. Wang and Liang [17] developed a multifault diagnosis method based on adaptive spectral Kurtosis analysis of the vibration signal. A theoretical model of multiple bearing faults was established in this paper. For the adaptive spectral Kurtosis technology, the main contribution was to determine the bandwidth and center frequency adaptively [18]. Tse and Wang [19] proposed a new method named sparsogram to quickly determine the resonant frequency bands. The sparsogram was constructed

using the sparsity measurements of the power spectra from the envelopes of wavelet packet coefficients at different WPD depths. Then, they presented an automatic selection process for finding the optimal complex Morlet wavelet filter with the help of genetic algorithm that maximizes the sparsity measurement value [20]. Liu et al. [21] proposed an adaptive spectral Kurtosis filtering based on Morlet wavelet and applied it to detect the signal transients.

However, Kurtosis also has its limitations for reflecting the impulse signals due to faults. For vibration time domain signals, single impulse produced by noise can have high Kurtosis value. However, the impulse signals repeat with specify frequency is the need signal. According to this, Kurtosis could have a false judgment in optimal frequency band selection. Similar to the Kurtosis of vibration time domain signals, Kurtosis of power spectrum also has its limitations. For bearing with severe stage faults, the fault frequency and its harmonics will dominate the whole spectrum shown in Figure 1. This represents the case of faulty bearing operating under relatively simple structure like electrical motor. For bearings in gearbox or bearings in other structures, especially for the incipient fault, the dominant frequency of power spectrum will not be the bearing fault frequency and its harmonics shown in Figure 2. In this case, the optimal frequency band cannot be determined through Kurtosis value of power spectrum. For bearing fault diagnosis inside the gearbox and its early stage of bearing fault, the dominant frequency in power spectrum will be the rotating frequency and mesh frequency of gear. However, compared to Kurtosis, the correlated Kurtosis (CK) developed by McDonald et al. [8] can detect the impulse signal according to the desired frequency and could be used to solve the above-mentioned problems. Compared to Kurtosis, CK mainly pays attention to the impulses repeated at a certain frequency (fault frequency). Therefore, it will not be affected by some noise similar to impulse. In gearbox, even if the impulses produced by gear fault are intense, CK only detect the desired impulses like bearing fault. CK takes advantage of the repetitiveness of the faults, and it is used in this work to detect impulses introduced by a faulted bearing [8]. It will be more precise than Kurtosis and can detect the weak signal produced by bearing incipient faults. In this paper, we used this indicator to select the optimal WPD node for bearing fault diagnosis.

In order to solve the above-mentioned dilemmas, time synchronous technology was used to delete the discrete frequency noise. This is very similar to another technique named blind source separation (BSS). For BSS technique, Bouguerriou et al. [22] proposed a new BSS algorithm based on the second statistical properties and applied it to the bearing defect diagnosis. Tse et al. [23] developed an enhanced eigenvector algorithm that consists of channel extension and a postprocessing method to recover multiple sources of vibrations. Wang and Tse [24] proposed a new blind component separation method which can decompose the mixed signal into two parts. They are periodic and transient subsets. The periodic subset is the signal related to the imbalance, misalignment, and eccentricity of a machine. The transient subset is the signal that refers to abnormal impulsive phenomena. Li et al. [25] put forward a new fault diagnosis

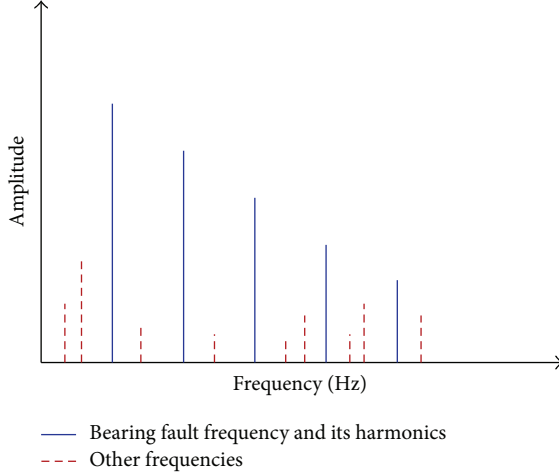


FIGURE 1: Schematic diagram of power spectrum of bearing fault (bearing fault frequency and its harmonics are dominant).

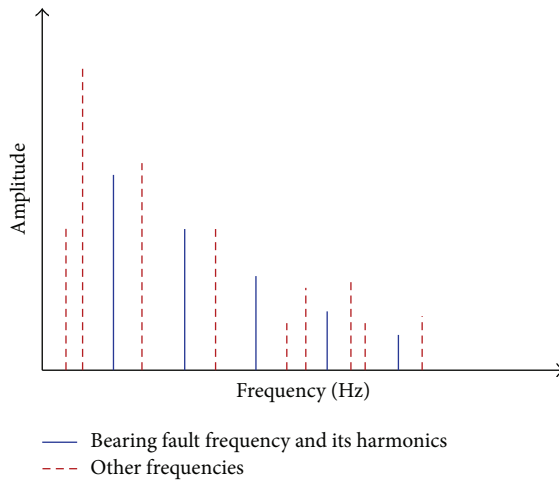


FIGURE 2: Schematic diagram of power spectrum of bearing fault (bearing fault frequency and its harmonics are undominant).

method for gearboxes based on the BSS and nonlinear feature extraction techniques. The kernel independent component analysis algorithm was used as the BSS method in the paper. Zhang et al. [26] proposed a fast BSS algorithm. A novel cost function was formulated for BSS through combining some kinds of temporal priori information. Keziou et al. [27] developed a new BSS approach by minimizing the empirical KL_m -divergence between copula densities. Hwang and Ho [28] proposed a novel operator-based model called the null space component analysis (NCA) to solve the noisy blind source separation problem. Compared to the ICA-based and the sparsity-based approaches, NCA is a deterministic and data-adaptive algorithm that can solve both the underdetermined and the overdetermined BSS problems. In contrast to the study of Lei et al. [12] and Wang et al. [13], after separation, WPD was used to decompose the bearing fault signals into different frequency band and CK was selected as an indicator to determine the optimal WPD node. Finally, power spectrum was applied to the envelope signal of optimal

node to find the bearing related fault frequencies. Two simulated bearing fault cases and three experimental bearing fault cases were used to demonstrate the effectiveness of proposed method.

The remainder of this paper is organized as follows. Section 2 put forward the new improved Kurtogram method for bearing fault detection. In Section 3, two simulated bearing fault data sets and three experimental bearing fault data sets from the laboratory are used to validate the proposed method. Simultaneously, comparison of proposed method and study of Lei et al. [12] and Wang et al. [13] has been investigated. Section 4 concludes the work.

2. Proposed Method for Bearing Fault Diagnosis

2.1. Brief Introduction to WPD. Suppose a space is \mathbf{V}_0 , and discrete wavelet only decomposes \mathbf{V}_0 to \mathbf{V}_1 and \mathbf{W}_1 . Then,

continue to decompose \mathbf{V}_1 to \mathbf{V}_2 and \mathbf{W}_2 , and so on. However, it does not decompose the \mathbf{W}_1 , and so forth. Whereas, WPD can further decompose the high frequency band (\mathbf{W}_j). So, the fault signal information of whole frequency band can be acquired through WPD. In general, a space \mathbf{V}_j of a multiresolution approximation is decomposed in a lower resolution space \mathbf{V}_{j+1} adding a detailed space \mathbf{W}_{j+1} . This is done through dividing the orthogonal basis $\{\phi_j(t - 2^j n)\}_{n \in \mathbb{Z}}$ of \mathbf{V}_j into two new orthogonal bases:

$$\begin{aligned} & \{\phi_{j+1}(t - 2^{j+1} n)\}_{n \in \mathbb{Z}} \text{ of } \mathbf{V}_{j+1}, \\ & \{\psi_{j+1}(t - 2^{j+1} n)\}_{n \in \mathbb{Z}} \text{ of } \mathbf{W}_{j+1}. \end{aligned} \quad (1)$$

Then, the decompositions of $\phi_{j+1,p} = \sum_{n=-\infty}^{+\infty} h[n-2p] \phi_{j,n}$ and $\psi_{j+1,p} = \sum_{n=-\infty}^{+\infty} g[n-2p] \phi_{j,n}$ of ϕ_{j+1} and ψ_{j+1} in the basis $\{\phi_j(t - 2^j n)\}_{n \in \mathbb{Z}}$ are specified by a pair of conjugate mirror filters $h[n]$ and $g[n] = (-1)^{1-n} h[1-n]$.

Then, a theorem was generalized.

Let $\{\theta_j(t - 2^j n)\}_{n \in \mathbb{Z}}$ be an orthonormal basis of a space \mathbf{U}_j . Let h and g be a pair of conjugate mirror filters. Define

$$\begin{aligned} \theta_{j+1}^0(t) &= \sum_{n=-\infty}^{+\infty} h[n] \theta_j(t - 2^j n), \\ \theta_{j+1}^1(t) &= \sum_{n=-\infty}^{+\infty} g[n] \theta_j(t - 2^j n). \end{aligned} \quad (2)$$

The family

$$\{\theta_{j+1}^0(t - 2^j n), \theta_{j+1}^1(t - 2^{j+1} n)\}_{n \in \mathbb{Z}} \quad (3)$$

is an orthonormal basis of \mathbf{U}_j . Because of the complex theory of WPD and limited pages, this is omitted in this paper.

WPD is actually a kind of wavelet transform where the signal is passed through more filters than the discrete wavelet transform. Usually, WPD can be represented as wavelet tree form. For example, three-level WPD is shown in Figure 3. Taking a bearing fault signal as an example, if the sampling frequency is F_s , three WPD depths will divide the frequency into 8 frequency bands. They are $0 F_s/16$ Hz, $F_s/16 F_s/8$ Hz, $F_s/8 - 3 F_s/16$ Hz, $3 F_s/16 F_s/4$ Hz, $F_s/4 - 5 F_s/16$ Hz, $5 F_s/16 - 3 F_s/8$ Hz, $3 F_s/8 - 7 F_s/16$ Hz, and $7 F_s/16 F_s/2$ Hz.

2.2. WPD Nodes Based Kurtogram. After WPD and reconstruction of node signal, a series of frequency band signals is acquired. Then, CK values of envelope signals can be calculated for each of the frequency band according to the following equation:

Correlated kurtosis of M -shift = $CK_M(\tau)$

$$= \frac{\sum_{t=1}^N \left(\prod_{m=0}^M y(t - m\tau) \right)^2}{\left(\sum_{t=1}^N y(t)^2 \right)^{M+1}}. \quad (4)$$

$y(t)$ is the envelope signal of reconstructed wavelet packet coefficient in this paper. τ is the interesting period of the fault. N is the number of samples in the input signal $y(t)$. If $\tau = 0$ and $M = 1$, this indeed is the traditional Kurtosis. It can detect the impulse signals effectively than traditional Kurtosis [8]. For example, if the desired frequency is 100 Hz and the sampling frequency is 12,000 Hz, the value of τ will be 120 samples. The flowchart of the new improved Kurtogram method in this paper is shown in Figure 4 and the detailed processes are described below.

- (1) The original accelerometer vibration signal and tachometer signal are used as input. In gearbox or other complex machineries, the vibration signals produced by bearing are very weak even if the bearing has faults. Time synchronous averaging (TSA) technique is used to reduce the nonsynchronous noise which mainly contains the random noise and bearing vibration signal. This is a well-known technique for gear and shaft fault diagnosis. On the contrary, it is possible to use this technique to separate the gear and shaft signal out in process of bearing fault diagnosis. Klein et al. [29] found that the residual signal (mainly containing the bearing fault signals) is possible to obtain using synchronous signals minus the TSA signals and proposed a novel method called the De-phase algorithm. The De-phase algorithm demonstrated a good performance to separate the bearing fault signals from the discrete frequencies (signals of shafts, gears, etc.).
- (2) WPD is used to decompose the residual signal at different depths for dividing the fault signal into different frequency bands. As declared in Wang et al., the minimum bandwidth decomposed by WPD at maximum depth needed to be three times longer than the desired fault frequency so that sufficient bearing fault-related signatures could be retained in the desired frequency band. This also can be regarded as a method to determine the maximum depth for WPD. After decomposition, the signals obtained at each specific node were reconstructed making it have the same temporal length as the original signal.
- (3) CK values of envelope signals of each node (frequency band) at different depth are calculated.

Then, the new improved Kurtogram can be obtained according to the work of Lei et al. The new improved Kurtogram is a colored map in which the depth of the color values is proportional to the CK values. Usually, only one optimal WPD node will be found. However, sometimes the bearing fault may have multiresonance frequencies. In this case, we need to analyze signals of first few maximum values. Finally, the power spectrums of envelope signals of selected frequency bands can be calculated and the bearing fault characteristic frequencies can be observed visually.

2.3. Main Differences between Proposed Method and Lei et al. and Wang et al. Methods. In this section, proposed method will be compared to other two previous developed Kurtogram

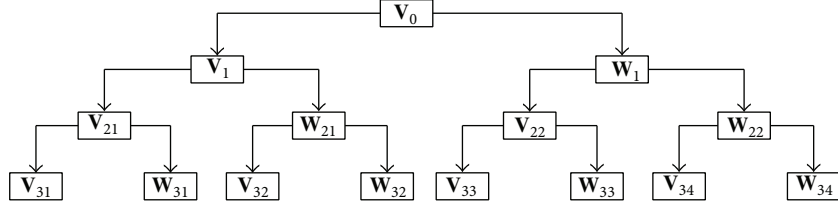


FIGURE 3: Three-level wavelet packet decomposition.

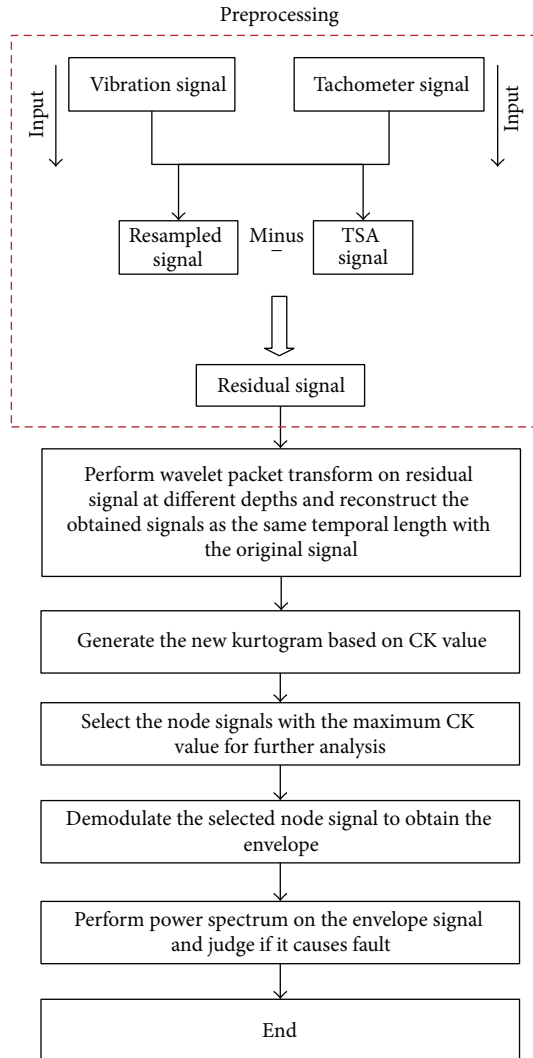


FIGURE 4: Flowchart of the proposed method.

methods of Lei et al. and Wang et al. Here, we reviewed the key steps of these two Kurtogram methods and declare the main difference with proposed method in this paper. Key steps of Kurtogram method proposed by Lei et al. are as follows.

- (1) WPD is used to decompose the signal in order to get a signal of different frequency bands.
- (2) Kurtosis values of each decomposed frequency band signals are calculated.

- (3) Kurtogram is formed using calculated Kurtosis values. Then, frequency band (WPD node) with highest Kurtosis value is selected for the envelope analysis.
- (4) Finally, the envelope spectrum is acquired to judge if it contains the bearing fault frequencies.

Key steps of Kurtogram method proposed in Wang et al. are as follows.

- (1) Autoregressive model (AR) is used for prewhitening the signal first. After this WPD is used to decompose

- the random signal. Similarly, a number of frequency bands signals are acquired.
- (2) Kurtosis values of power spectrum of envelope of each decomposed frequency band signals are calculated.
 - (3) Kurtogram is formed using calculated Kurtosis values. Similarly, frequency band with maximum Kurtosis value is selected for the envelope analysis.
 - (4) Finally, the power spectrum of envelope signals is acquired to judge if it contains the bearing fault frequencies.

There are two main differences between proposed method in this paper and method by Lei et al. *First*, method of Lei et al. directly decomposes the fault signal using WPD, while the proposed method in this paper first separates the bearing fault signals from discrete frequency and noise using De-phase algorithm in order to get a residual signal. Then, residual signal is used as input for the decomposition. *Second*, method of Lei et al. calculates Kurtosis values of decomposed node signals which are implemented in time domain, while the proposed method in this paper calculates CK values of envelope decomposed node signals. Similarly, there are two main differences between proposed method in this paper and method by Wang et al. *First*, method of Wang et al. use AR model to extract bearing fault signals, while the proposed method uses De-phase algorithm for it. *Second*, method of Wang et al. calculates Kurtosis values of envelope spectrums of decomposed node signals which are conducted in frequency domain, while the proposed method in this paper calculates CK values of envelope decomposed node signals.

3. The Proposed Method Validated by Simulated and Experimental Case Studies

3.1. Case 1: Simulated Bearing Fault Signals with Single Resonant Frequency. First, signals with single resonant frequency under different SNR were considered. Similar to Lei et al. and Wang et al. work [12, 13], Daubechies 10 wavelet was used in proposed method to decompose the signal. The simulated signal with single resonant frequency is given as

$$y(t) = y_0 e^{-\xi \times 2\pi f_n \times t - \tau} \sin \left(2\pi f_n \times \sqrt{1 - \xi^2} \times t - \tau \right), \quad (5)$$

where ξ is equal to 0.1, f_n is the resonant frequency equal to 1,700 Hz, and τ is used to simulate the randomness caused by slippage which is subject to a discrete uniform distribution. y_0 (equal to one) is the amplitude of simulated bearing impulse signal. Suppose the sampling frequency is 12,000 Hz. Then, we can simulate the bearing fault signals according to fault frequency (equal to 100 Hz). A total of 24,000 samplings were used for each simulated signal. Finally, a random signal with a mean of zero and a standard deviation of 0.1 were added to (5).

Figures 5(a)–5(c) show simulated signal, noise signal, and mixed signal. The proposed method was used to analyze the mixed signal shown in Figure 5(c). The new improved

Kurtogram is shown in Figure 6(a). As shown, node (1, 1) has the highest CK value of all nodes. Then, the signal of node (1, 1) was reconstructed. The power spectrum of the envelope signal extracted from node (1, 1) by WPD is given in Figure 6(b), in which the fault frequency, 100 Hz, and its harmonics are obvious. It should be noted that the CK value was calculated based on the desired period of bearing fault. For this simulated signal, the period of fault is 120 samples (corresponding to the τ in (4)). In this case, the parameter M of CK equals 15.

Beside of this, the improved Kurtogram proposed by Lei et al. and enhanced Kurtogram proposed by Wang et al. are applied to analyze the same mixed signal with one resonant frequency in the case of the same noise level of 0.1. Their performance is given in Figures 7 and 8. It can be found that Lei et al. improved Kurtogram has the same diagnosis result with proposed method in this paper. Wang et al. enhanced Kurtogram result is shown in Figure 8. The amplitudes of fault frequency and its harmonics are smaller compared to those determined by the proposed new improved Kurtogram in this paper.

Next, we increased the noise level to 0.5 and analyze the mixed signal. The results can be seen in Figures 9–11. The result of new improved Kurtogram is shown in Figure 9 and it is possible to see the obvious fault frequency and its harmonics. However, it can be found that Lei et al. improved Kurtogram fail to detect the single resonant frequency node. In addition, compared to Figure 9, the harmonics amplitudes of fault characteristics frequency of 100 Hz in this case, shown in Figure 11, are smaller. This confirms that the proposed new improved Kurtogram is superior to the enhanced Kurtogram proposed by Wang et al.

Afterwards, we continue to decrease the SNR of simulated bearing fault signal. We add a random Gaussian noise with zero mean and standard deviation 0.8 to the impulse signal. Then, we compare the performance of three Kurtograms. The result of the new improved Kurtogram is shown in Figure 12(a). Node (3, 4) is selected as the optimal node which contains bearing fault information. Similarly, the power spectrum of the envelope signal extracted from the reconstructed signal of node (3, 4) is given in Figure 12(b). We can see that the fault frequency and its second and third harmonics are very clear. Compared to the noise level 0.5, the optimal frequency band determined by new improved Kurtogram is the same. The optimal frequency band and its power spectrum determined by Lei et al. and Wang et al. Kurtogram are shown in Figures 13 and 14. According to this both methods fail to detect the bearing fault frequency, though, for the noise level of 0.5, Kurtogram developed by Wang et al. can detect the bearing fault effectively. However, when the impulsive signal of bearing fault mixed with strong noise, the Wang et al. Kurtogram loses its primary goal. On the contrary, the new improved Kurtogram based on the CK value can diagnose the bearing fault even if the SNR is very low, noise level of 0.8.

When the noise level is 0.1, the resonance frequency falls in the optimal frequency band determined by proposed Kurtogram and Lei et al. improved Kurtogram methods. This is because of the low noise level. When the noise level

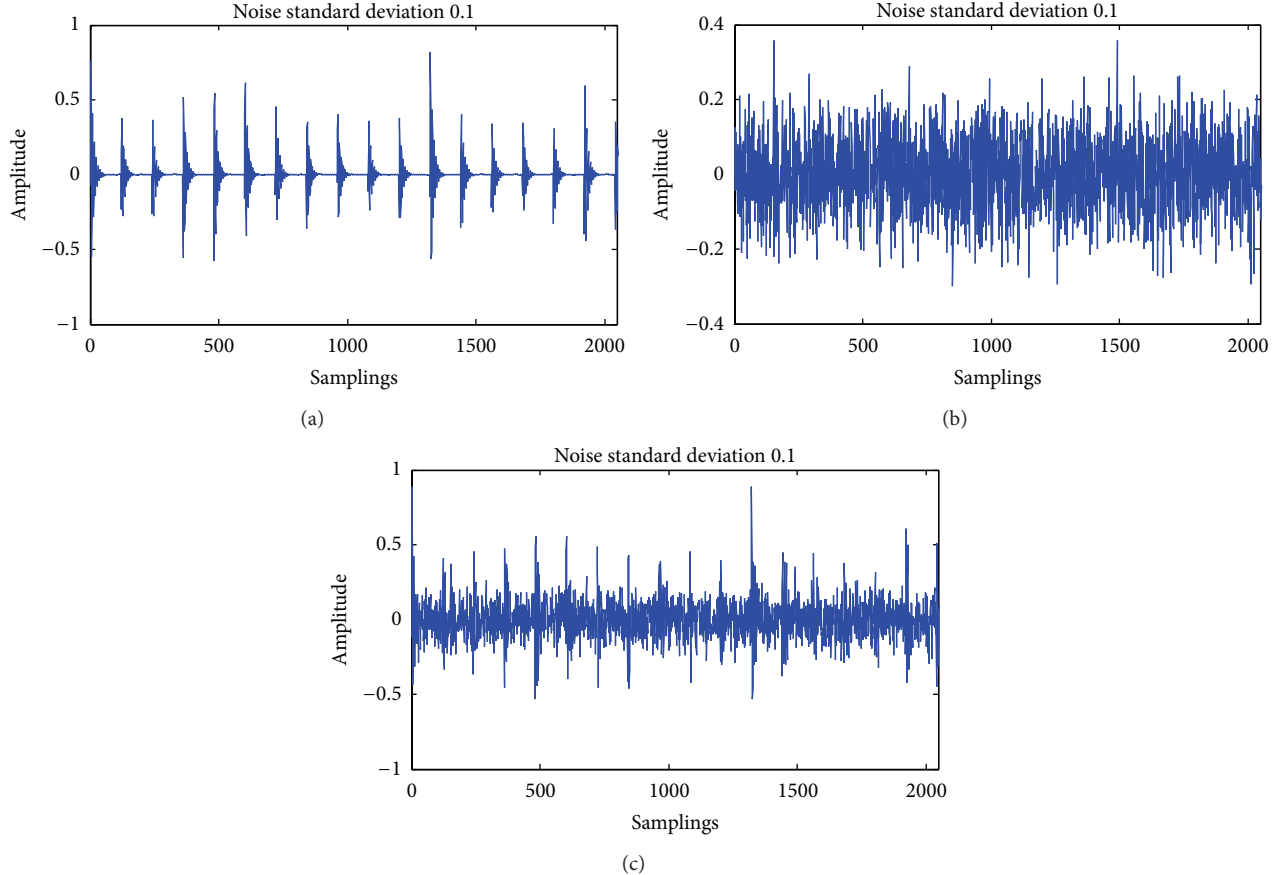


FIGURE 5: Simulated time domain signal: (a) simulated impulse signal with one resonance frequency, (b) the noise signal with zero mean and standard deviation of 0.1, and (c) the finally mixed signal.

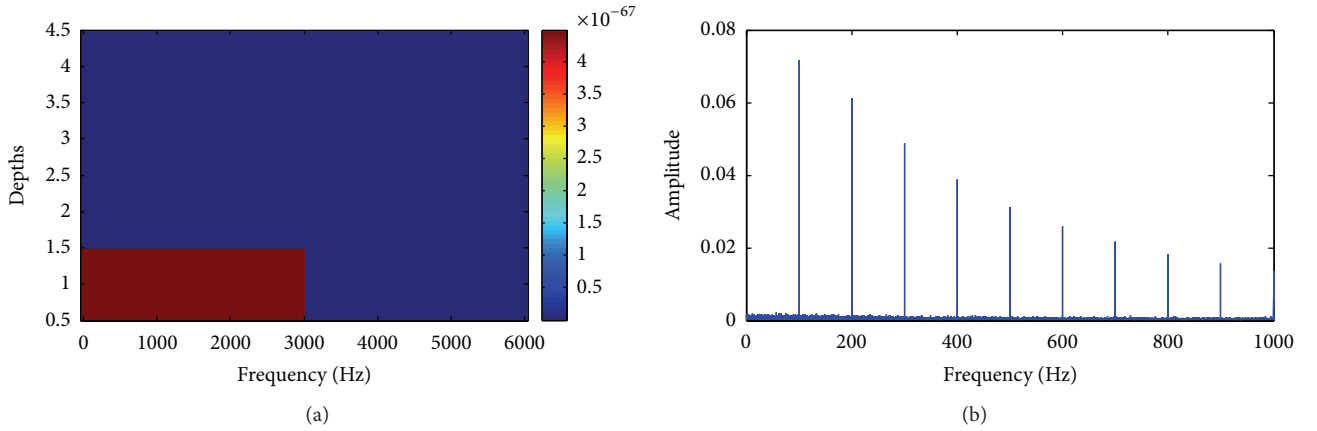


FIGURE 6: The results obtained by the proposed method for processing the mixed signal with one resonant frequency. (a) The new improved Kurtogram and (b) power spectrum of the envelope of the signal extracted from node (1, 1) by WPD.

is increased, the reconstructed signal of different frequency band may be distorted by noise or the inherent deficiencies of WPD and reconstruction process. This will lead to the frequency band containing the resonant frequency without biggest impulsive signal. Therefore, in the case with noise

level of 0.5 and 0.8, the best frequency band determined by new improved Kurtogram does not contain the 1,700 Hz.

3.2. Case 2: Simulated Bearing Fault Signals with an Interference. In industrial application, bearings always operate

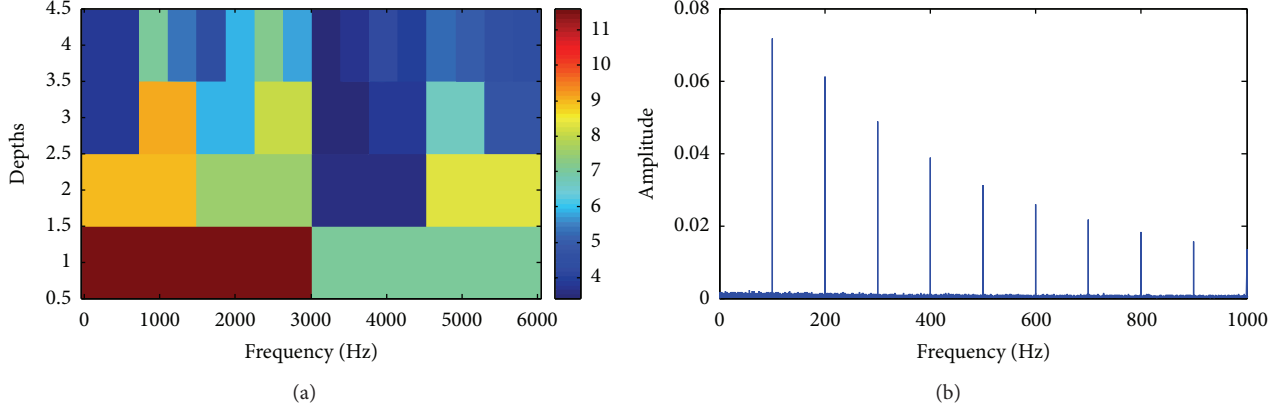


FIGURE 7: The results obtained by the improved Kurtogram proposed by Lei et al. for processing the mixed signal with one resonant frequency. (a) The improved Kurtogram and (b) power spectrum of the envelope of the signal extracted from node (1, 1) by WPD.

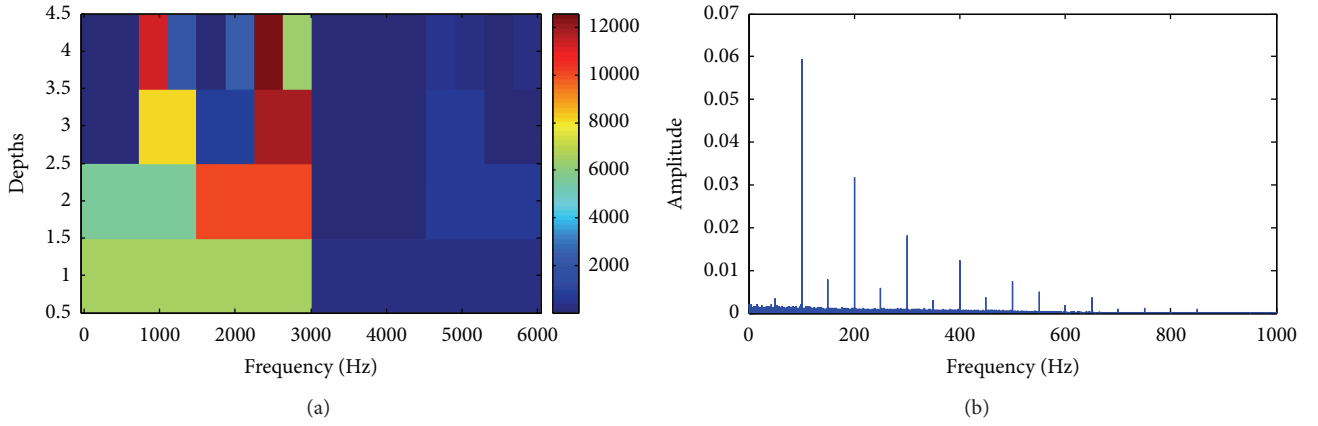


FIGURE 8: The results obtained by the enhanced Kurtogram proposed by Wang et al. for processing the mixed signal with one resonance frequency. (a) The enhanced Kurtogram and (b) power spectrum of the envelope of the signal extracted from node (4, 7) by WPD.

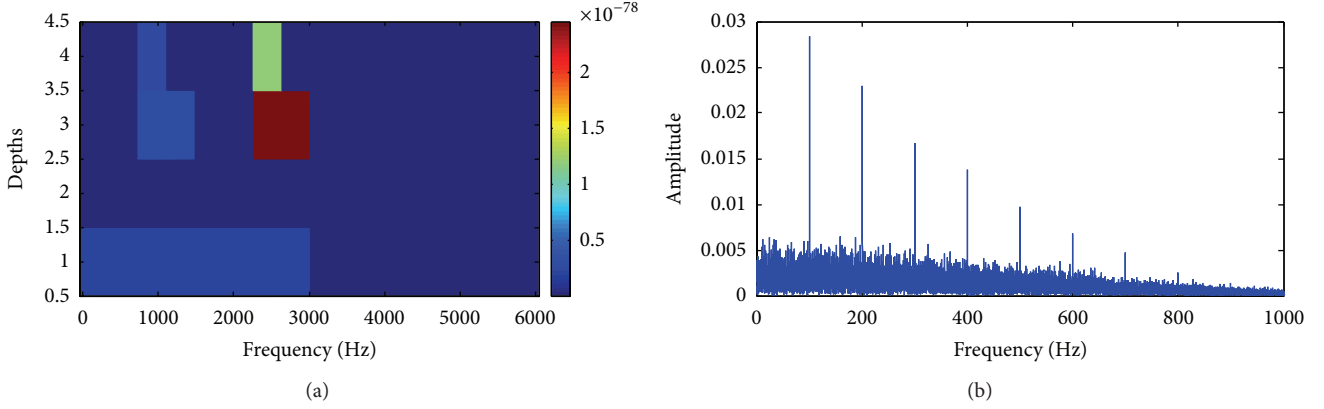


FIGURE 9: The results obtained by the proposed method for processing the mixed signal with one resonant frequency. (a) The new improved Kurtogram and (b) power spectrum of the envelope of the signal extracted from node (3, 4) by WPD.

together with other components like gears and shafts and because this vibration signal usually contains broad range of frequencies. In the process of bearing fault diagnosis, those other frequencies are called interference frequencies. For the evaluation of performance of new improved Kurtogram, we

add another interference frequency of 13 Hz with resonant frequency at 600 Hz. The amplitude of 13 Hz frequency in this case was set to 5. This means this frequency has more intensity than desired bearing fault frequency 100 Hz with amplitude of 1. The standard deviation of added noise is 0.5. Similar

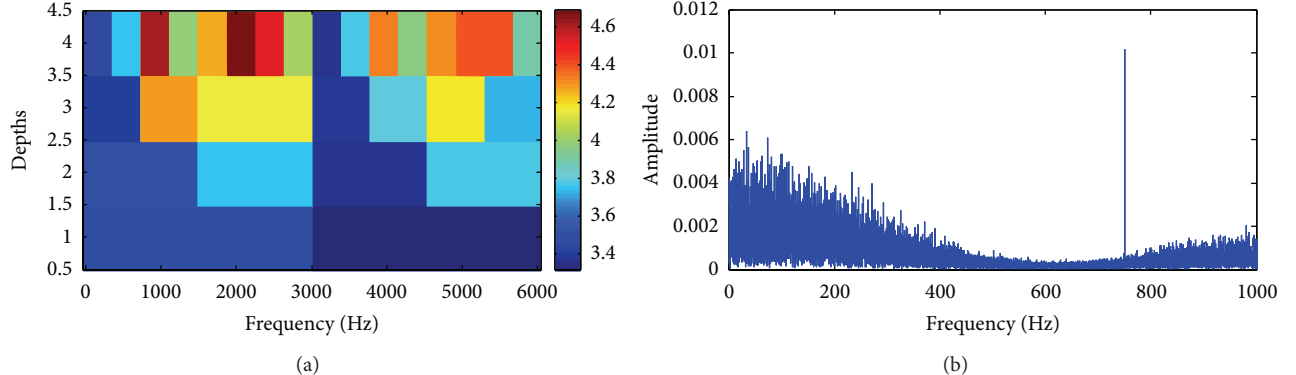


FIGURE 10: The results obtained by the improved Kurtogram proposed by Lei et al. for processing the mixed signal with one resonant frequency. (a) The improved Kurtogram and (b) power spectrum of the envelope of the signal extracted from node (4, 6) by WPD.

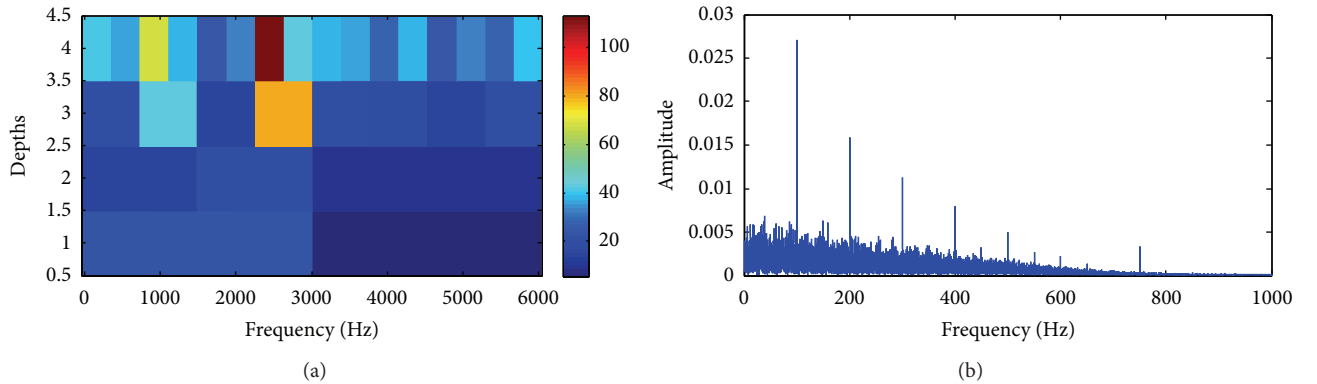


FIGURE 11: The results obtained by the enhanced Kurtogram proposed by Wang et al. for processing the mixed signal with one resonant frequency. (a) The enhanced Kurtogram and (b) power spectrum of the envelope of the signal extracted from node (4, 7) by WPD.

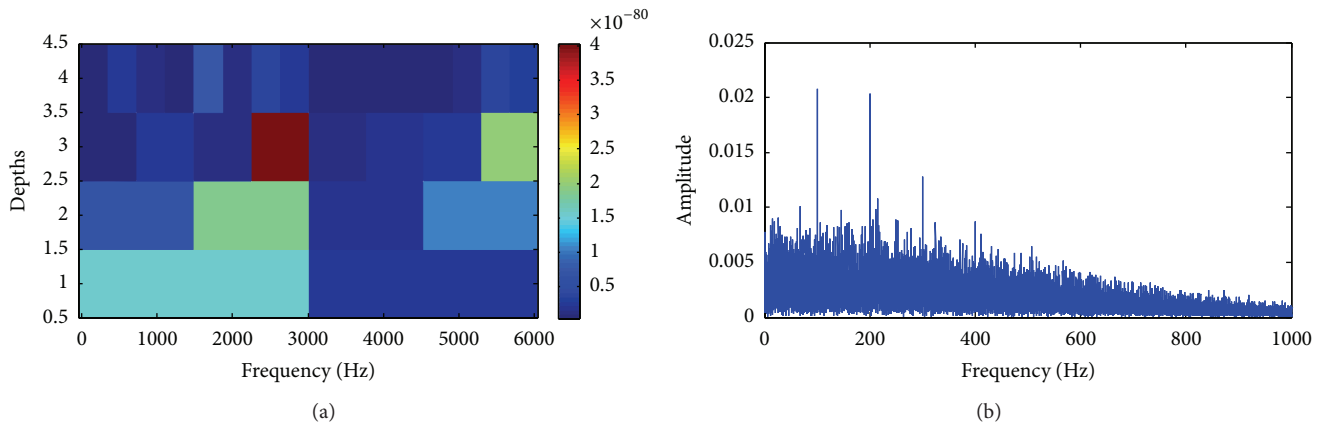


FIGURE 12: The results obtained by the proposed method for processing the mixed signal with one resonant frequency under the noise level 0.8. (a) The new improved Kurtogram and (b) power spectrum of the envelope of the signal extracted from node (3, 4) by WPD.

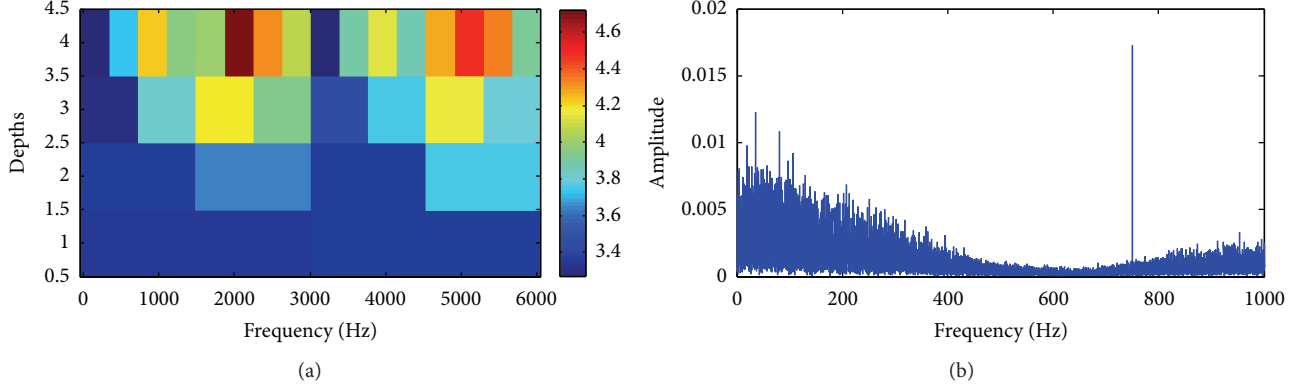


FIGURE 13: The results obtained by the improved Kurtogram proposed by Lei et al. for processing the mixed signal with one resonant frequency under noise level of 0.8. (a) The improved Kurtogram and (b) power spectrum of the envelope of the signal extracted from node (4, 6) by WPD.

TABLE 1: Characteristic frequencies of bearings (Hz).

| Bearing type | BPFO | BPFI | BSF | FTF |
|--------------|-------|--------|-------|-------|
| RBC NICE | 81.12 | 118.88 | 63.86 | 10.14 |

to analysis of Case 1, the performance of three Kurtogram methods are evaluated. The Kurtograms and related power spectrums are shown in Figures 15–17. We can see that both Lei et al. and Wang et al. methods only can detect the 13 Hz interference frequency. However, the proposed new improved Kurtogram based on CK can detect the desired bearing fault frequency and its harmonics. This case study further demonstrates the superiority of proposed method to the other two methods. In this case, the value of M is 15.

3.3. Case 3: Experimental Case Studies. The vibration fault data set used in this case study was obtained from the Mechanical Failures Prevention Group (MFPT) assembled and prepared on behalf of MFPT by Dr. Bechhoefer [30]. Only the outer race and inner race faults are considered for evaluation and discussion it this study. Bearing faults are implanted artificially. The test bearing which supports the motor shaft is radial ball bearings produced by RBC NICE with following parameters: roller diameter 71.628 mm, pitch diameter 379.476 mm, number of elements is 8, and the contact angle equal to 0° . In this case study data set with 25 Hz input shaft rate, 48,828 Hz sampling frequency, 3 s sampling duration, and 50 lbs. load is used. If we define the four bearing fault frequencies as ball pass frequency inner race (BPFI), ball pass frequency outer race (BPFO), ball spin frequency (BSF), and fundamental train frequency (FTF), fault frequencies could be calculated according to the geometric parameters [31] shown in Table 1.

3.3.1. Outer Race Fault Analysis. According to the framework of proposed method shown in Figure 4, the results are acquired. As shown in Figure 18(a), the optimal WPD node containing the impulsive signal produced by bearing fault

is (3, 7). From the power spectrum shown in Figure 18(b), we can see that the BPFO and its harmonics are very clear. This demonstrates the effectiveness of proposed method with value of M being equal to 2.

Similarly, the results of Lei et al. and Wang et al. methods are shown in Figures 19 and 20, respectively. Application results show that these two methods can diagnose the outer race fault effectively. In these three methods, Lei et al. method has shown the best result because the BPFO fault frequency and its harmonics are clearer than that of Wang et al. method and the proposed method in this paper.

3.3.2. Inner Race Fault Analysis. Similar to the outer race fault analysis, the results of three Kurtogram methods are shown in Figures 21–23. Comparing these results, it shows that new improved Kurtogram method is superior to the other two methods. The BPFI and its harmonics are very clear in power spectrum compared to Lei et al. and Wang et al. methods with value of M being equal to 2.

3.4. Case 4: Implanted Bearing Outer Race Fault in Gearbox. A complete description of the test-rig and instrumentation can be found in [32] and only a brief review of the experimental testing is provided here. The power to one stage gearbox type ZD10 is provided by a three-phase asynchronous motor type YCT180-4A. The motor speed can be adjusted by a speed controller, provided an option for testing under different speed and load. A water cooled magnetic powder brake FZJ-5 connected to the output shaft is used to provide load for gearbox. The torque can be controlled by different DC power of the brake. Two speed and torque sensors are used for record the speed and torque information related to the input shaft and output shaft, respectively. Speed sensor produces 60 impulses per revolution. Input shaft is supported by 6206 and output shaft by 7207 bearings. Gear on input shaft has 30 teeth and meshes with gear on output shaft which has 50 teeth. Input shaft rotating frequency is 19.60 Hz, which gives 588 Hz the meshing frequency.

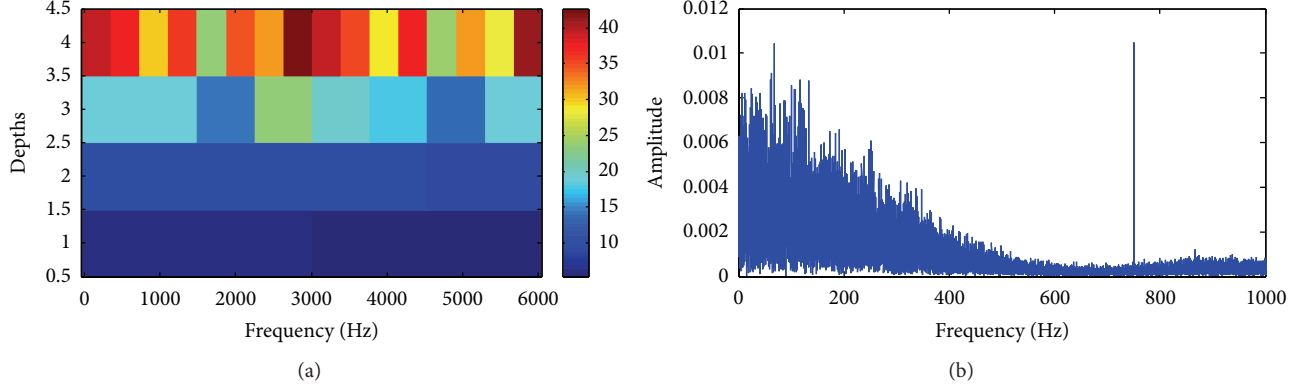


FIGURE 14: The results obtained by the enhanced Kurtogram proposed by Wang et al. for processing the mixed signal with one resonance frequency under noise level of 0.8. (a) The enhanced Kurtogram and (b) power spectrum of the envelope of the signal extracted from node (4, 8) by WPD.

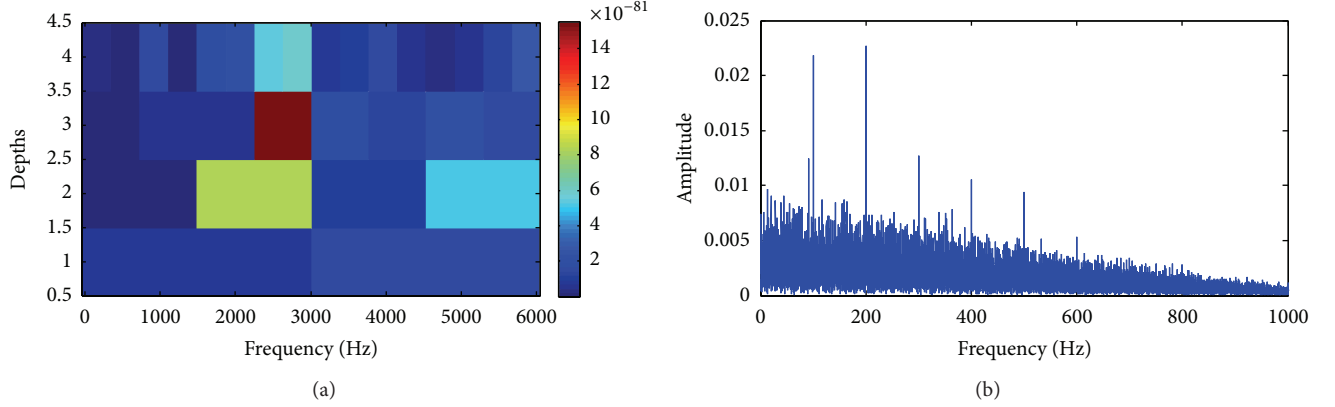


FIGURE 15: The results obtained by the proposed method for processing the mixed signal with interference frequency under noise level of 0.5. (a) The new improved Kurtogram and (b) power spectrum of the envelope of the signal extracted from node (3, 4) by WPD.

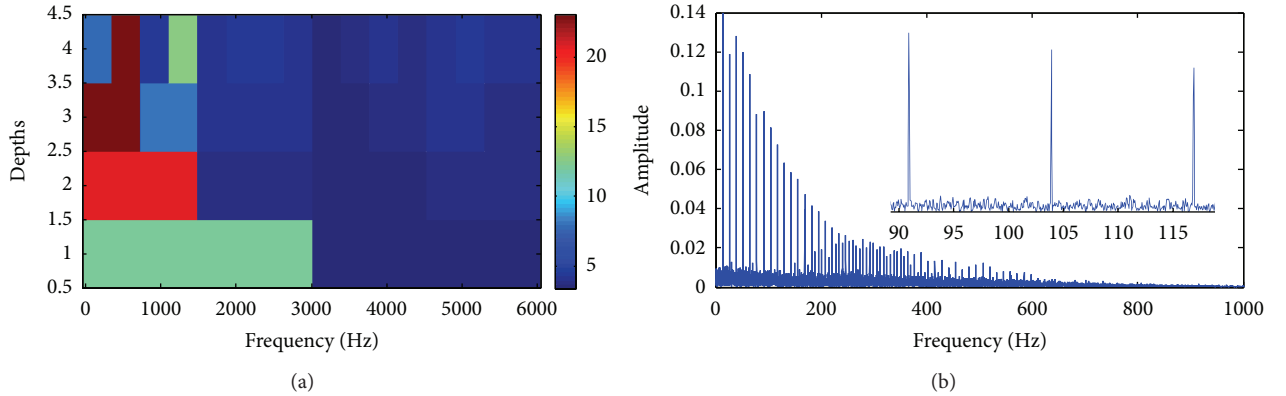


FIGURE 16: The results obtained by the improved Kurtogram proposed by Lei et al. for processing the mixed signal with interference frequency under noise level of 0.5. (a) The improved Kurtogram and (b) power spectrum of the envelope of the signal extracted from node (4, 2) by WPD.

The artificial fault was 0.5 mm width, 1.5 mm depth on groove, which was cut on the outer race of input shaft bearing (6206) using wire-electrode cutting. The sampling frequency was 12,800 Hz and the sampling time was 2.56 seconds. Characteristic fault frequencies for bearing 6206 bearings under

1 Hz shaft rate are (BPFO, 3.5806 Hz), (BPFI 5.4194 Hz), (BSF, 2.3452 Hz), and (FTF, 0.3978 Hz). For 19.60 Hz input shaft rotating frequency BPFO is 70.2 Hz.

Different from the previous case studies, the bearing fault signal in this case has interference from the gear and

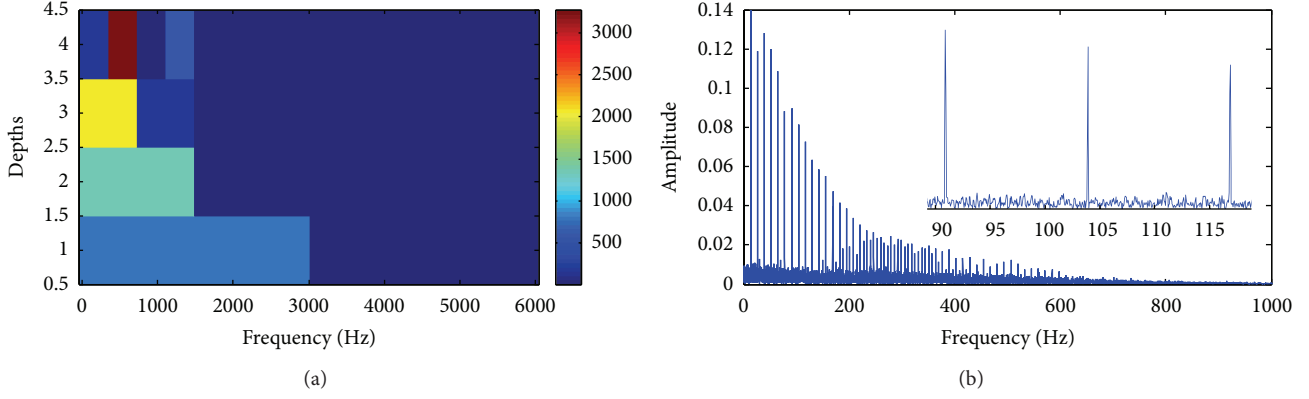


FIGURE 17: The results obtained by the enhanced Kurtogram proposed by Wang et al. for processing the mixed signal with interference frequency under noise level of 0.5. (a) The enhanced Kurtogram and (b) power spectrum of the envelope of the signal extracted from node (4, 2) by WPD.

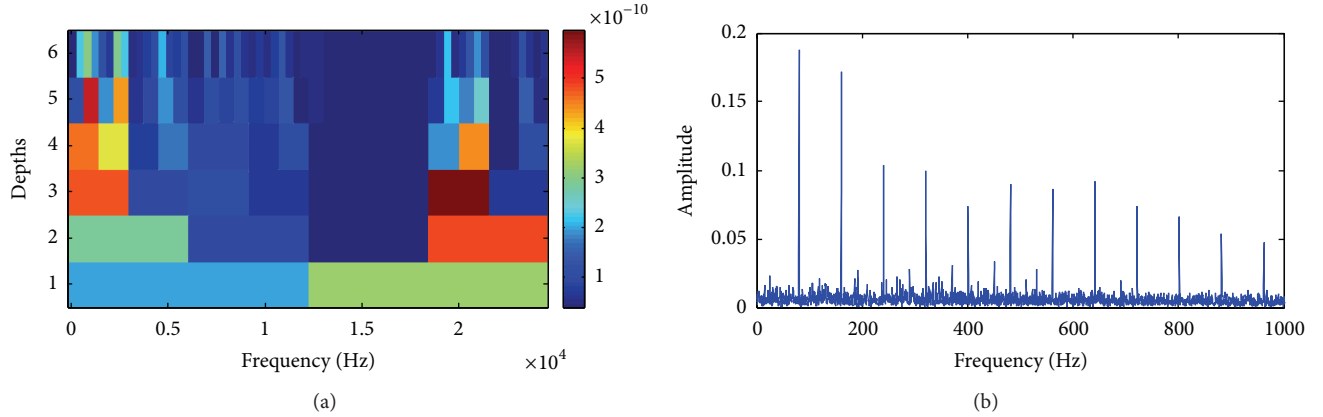


FIGURE 18: The results obtained by the proposed method for processing the outer race fault of NICE bearing. (a) The new improved Kurtogram and (b) power spectrum of the envelope of the signal extracted from node (3, 7) by WPD.

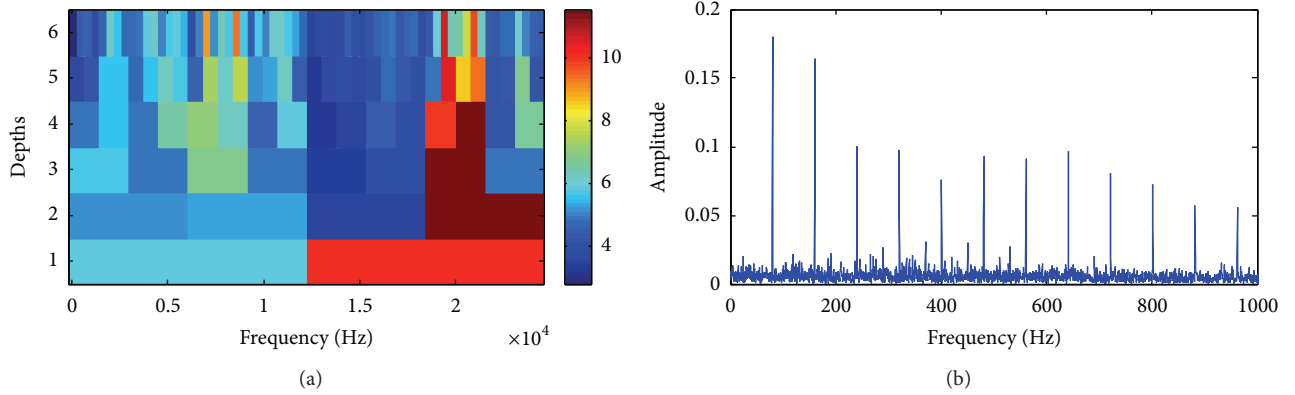


FIGURE 19: The results obtained by the improved Kurtogram proposed by Lei et al. for processing the outer race fault of NICE bearing. (a) The improved Kurtogram and (b) power spectrum of the envelope of the signal extracted from node (4, 14) by WPD.

shaft vibration and we acquired the residual signal using De-phase algorithm for prewhitening. After this we compared new improved Kurtogram with other ones mentioned earlier. Testing results are shown in Figures 24–26. It shows the optimal frequency band determined by Lei et al. and Wang

et al. methods providing the same results. From the power spectrum, the BPFO fault frequency and its harmonics can be found. However, the optimal frequency band determined by new improved Kurtogram in this paper has better effect because the BPFO fault frequency and its harmonics in

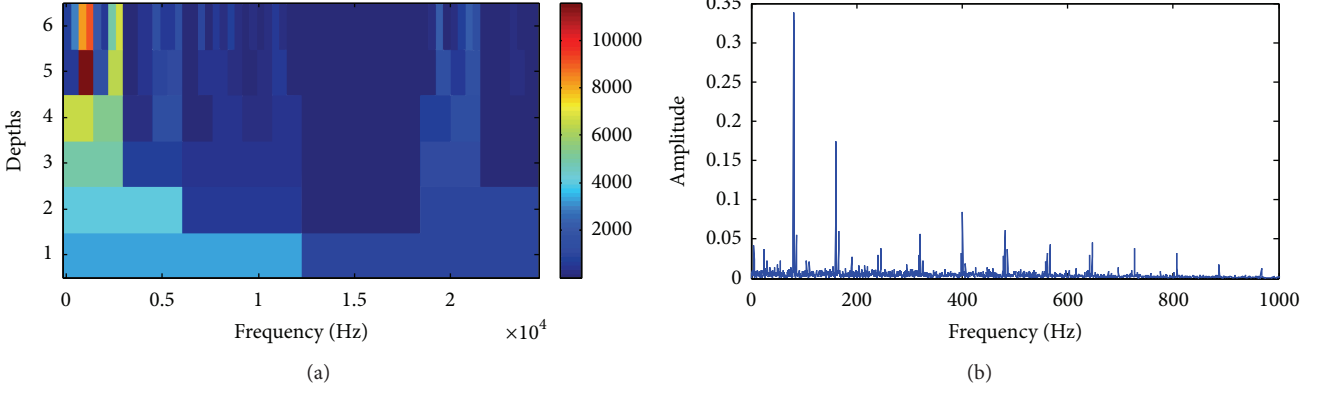


FIGURE 20: The results obtained by the enhanced Kurtogram proposed by Wang et al. for processing the outer race fault of NICE bearing. (a) The enhanced Kurtogram and (b) power spectrum of the envelope of the signal extracted from node (5, 2) by WPD.

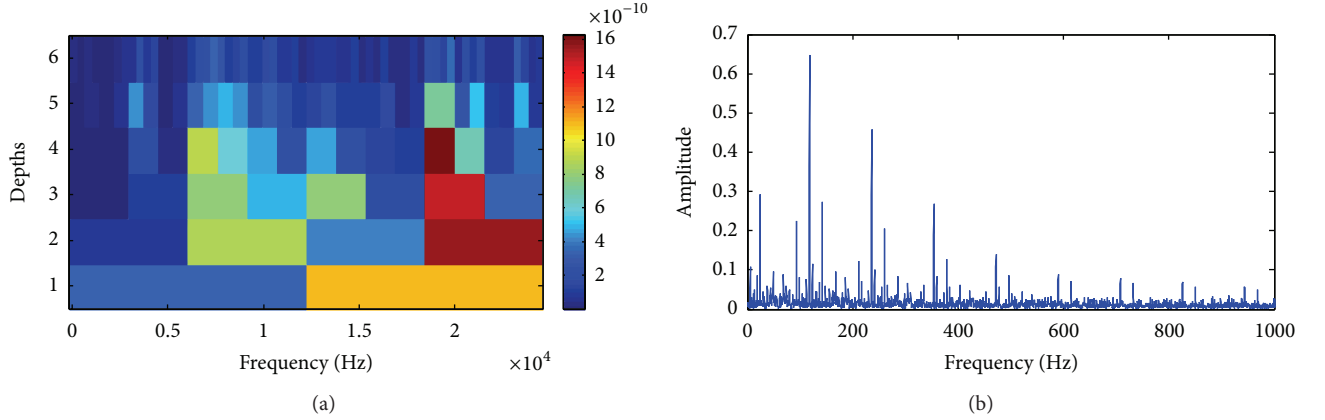


FIGURE 21: The results obtained by the proposed method for processing the inner race fault of NICE bearing. (a) The new improved Kurtogram and (b) power spectrum of the envelope of the signal extracted from node (4, 13) by WPD.

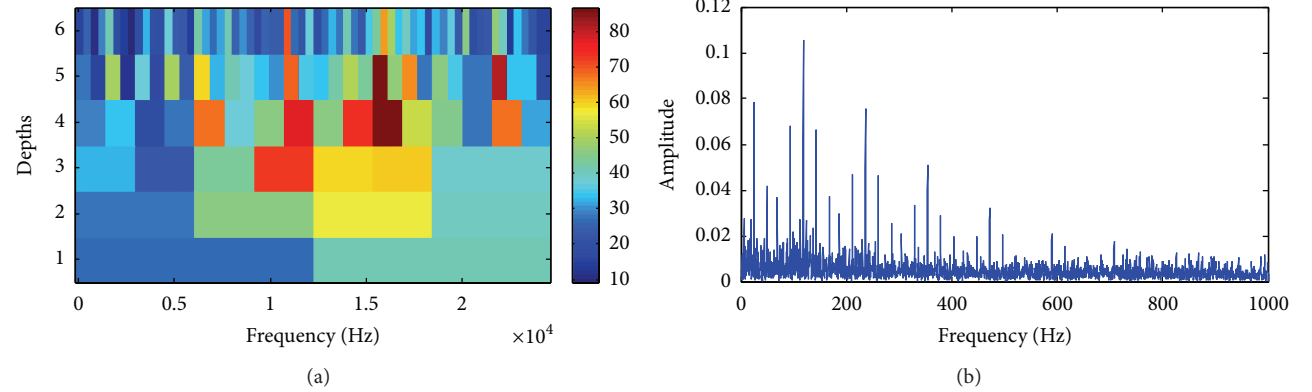


FIGURE 22: The results obtained by the improved Kurtogram proposed by lei et al. for processing the inner race fault of NICE bearing. (a) The improved Kurtogram and (b) power spectrum of the envelope of the signal extracted from node (5, 21) by WPD.

envelope spectrum have higher amplitude compared with other two methods, with value of M being equal to 15.

3.5. Case 5: Naturally Developed Multifault of Bearing in Gearbox. It is necessary to say that this experiment is not an implanted fault test. The bearing faults were progressed

naturally with the gear full life test [33]. In order to research the weak signal diagnosis method, we acquired the vibration signal again after adjusting the transducers' location. In the full life test, all the gears in this gearbox had different level of wear. After test, the bearings in this gearbox are cut into halves to observe the defects. Figure 27 shows the experimental

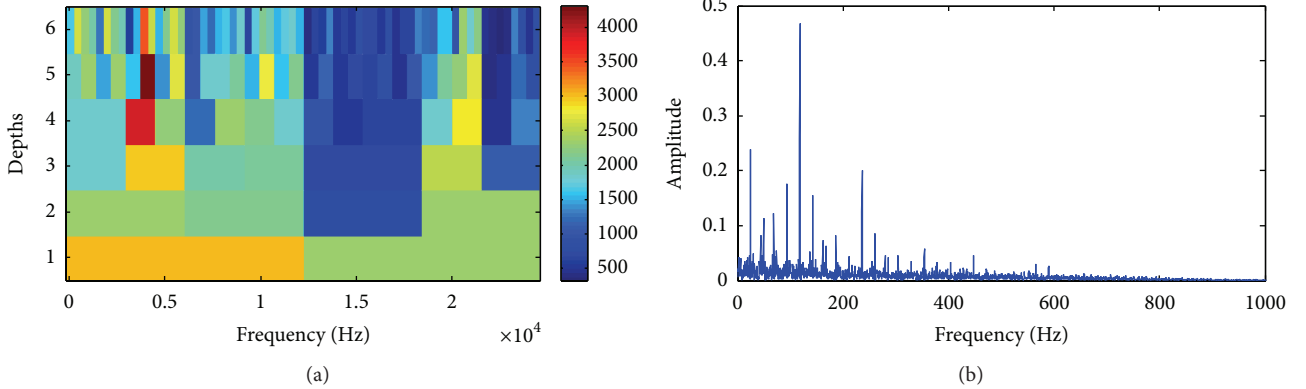


FIGURE 23: The results obtained by the enhanced Kurtogram proposed by Wang et al. for processing the inner race fault of NICE bearing. (a) The enhanced Kurtogram and (b) power spectrum of the envelope of the signal extracted from node (5, 6) by WPD.

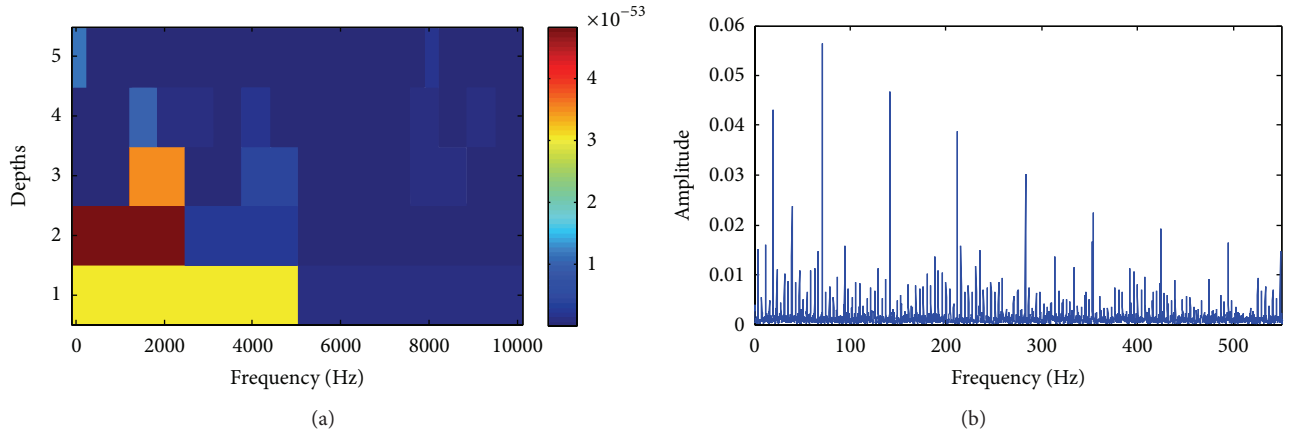


FIGURE 24: The results obtained by the proposed method for processing the outer race fault of 6206 bearing in gearbox. (a) The new improved Kurtogram and (b) power spectrum of the envelope of the signal extracted from node (2, 1) by WPD.

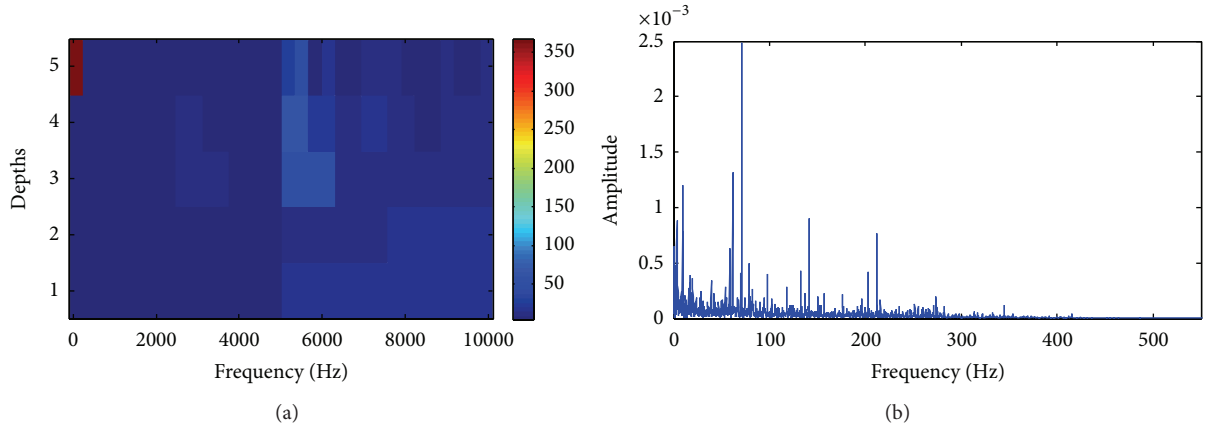


FIGURE 25: The results obtained by the improved Kurtogram proposed by Lei et al. for processing the outer race fault of 6206 bearing in gearbox. (a) The improved Kurtogram and (b) power spectrum of the envelope of the signal extracted from node (5, 1) by WPD.

test rig used in this paper to verify the performance of the proposed method. It contains a gearbox, a 4 kW three-phase asynchronous motor for driving the gearbox, and a magnetic powder brake for loading. The motor allows the

tested gear to operate under various speeds. The load is provided by the magnetic powder brake connected to the output shaft and the torque can be adjusted by a brake controller. The gearbox has three shafts, which are mounted

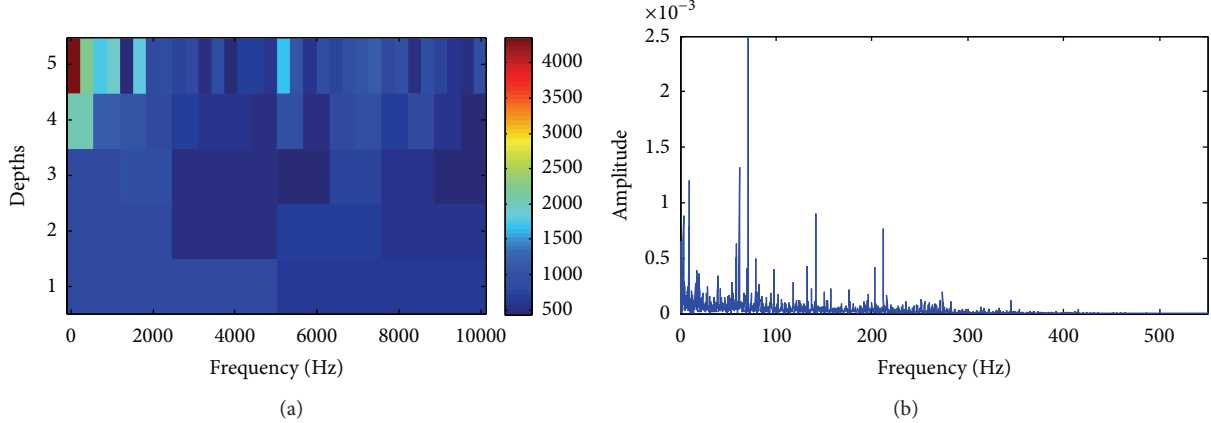


FIGURE 26: The results obtained by the enhanced Kurtogram proposed by Wang et al. for processing the outer race fault of 6206 bearing in gearbox. (a) The enhanced Kurtogram and (b) power spectrum of the envelope of the signal extracted from node (5, 1) by WPD.

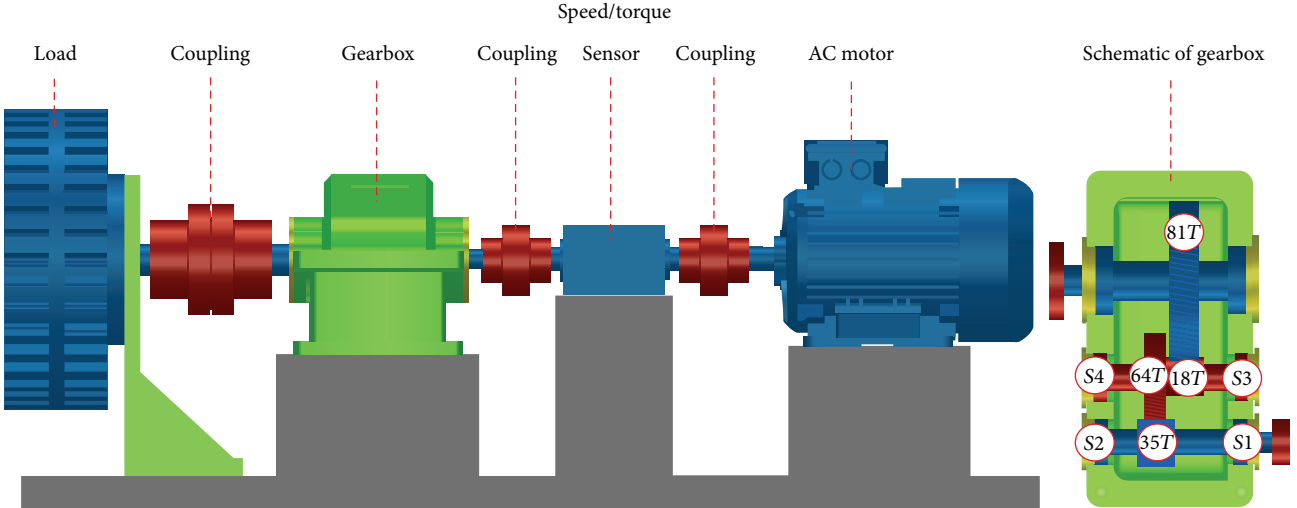


FIGURE 27: A schematic of the experimental two-stage gearbox test rig.

to the gearbox housing by bearings. Gear 1 on low speed (LS) shaft has 81 teeth and meshes with gear 3 with 18 teeth. Gear 2 on intermediate speed (IS) shaft has 64 teeth and meshes with gear 4, which is on the high speed (HS) shaft and has 35 teeth. In order to acquire the speed and torque information, a speed and torque transducer is installed on the HS shaft. Four accelerometers were mounted on the top of the gearbox casing and the vibration signals were collected from accelerometer at position S1.

During bearing inspection, we found that all the bearings have different faults level. Because of the page limitation, only bearings on high speed shaft were selected as the analyzing object. The bearing of left side has outer race fault as shown in Figure 28(a). The bearing of right side has outer race fault, inner race fault, and ball fault as shown in Figures 28(b) and 29. In this case, only HS bearing faults under load 0 Nm and 405 Nm are considered.

3.5.1. Results of Bearing Faults under Load 0 Nm. Similar to Case 4, the residual signal is acquired using De-phase algorithm. Then, three different Kurtogram methods are applied to the residual signal. The results are shown in Figures 30–34. In this case, the value of M is 15. Because this case has three fault types, so we need three different CK to detect the corresponding fault. In other words, the τ of CK is different for different fault type. The four base fault frequencies (1 Hz shaft rate) are (BPFO, 3.585), (BPFI, 5.415), (BSF, 2.357), and (FTF, 0.398). In this case input shaft speed was 20.0222 Hz. Therefore, the fault frequencies are (BPFO, 71.78 Hz), (BPFI, 108.4 Hz), and (BSF, 47.19 Hz). From Figure 30, we can see that the outer race fault is detected effectively. The BPFO and its second and third harmonics are very clear. Similar to the outer race fault detection, the BPFI and its second harmonic are clear in Figure 31. However, we cannot find the BSF and its harmonics from Figure 32. Compared with method proposed

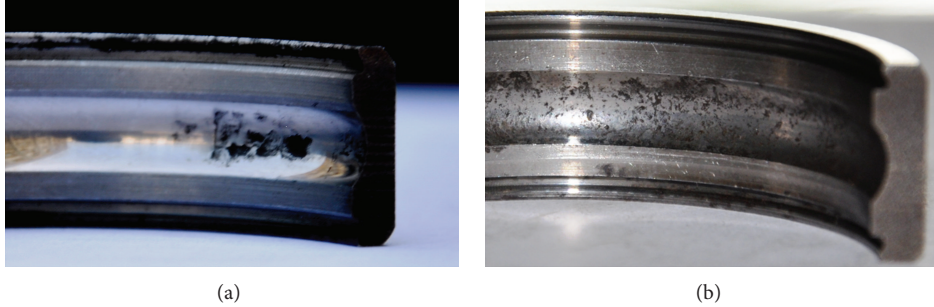


FIGURE 28: HS shaft bearing BPFO faults: (a) left bearing and (b) right bearing.



FIGURE 29: HS right bearing faults: (a) BPFI and (b) BSF.

in this paper, improved Kurtogram developed by Lei et al. and enhanced Kurtogram developed by Wang et al. cannot detect the bearing faults.

3.5.2. Results of Bearing Faults under Load 405 Nm. Similar to case study under load 0 Nm, the results of three Kurtogram methods are shown in Figures 35–39. In this case, the value of M was 15. Input shaft speed was 19.66 Hz and bearing fault frequencies are (BPFO, 70.5 Hz), (BPFI, 106.5 Hz), and (BSF, 46.35 Hz). From Figures 35–37, we can see that outer race and inner race faults can be detected; however, the ball fault is missed. Figure 38 shows that improved Kurtogram method developed by Lei et al. can both detect the outer race and inner race faults. Similar to the new improved Kurtogram method, the ball fault is undetected. However, the enhanced Kurtogram developed by Wang et al. cannot detect any of bearing faults.

3.6. Discussions. In this paper, using five case studies, we demonstrated the effectiveness of proposed method. However, there are some issues which should be further discussed.

(1) The bearings always operate with other components simultaneously and the bearing faulty signals often interfere by other components. As we know, the signature of faulty bearings in electric motor are relatively simple compared to the signal of faulty bearings in gearbox. This is why Wang et al. enhanced Kurtogram method is useful for motor bearing fault

diagnosis other than gearbox bearing fault diagnosis (Case 5).

- (2) Unlike the implanted bearing faults, naturally developed bearing faults are very weak and sometimes those are the distributed faults (like Figure 30). This is why proposed new improved Kurtogram gives good results in Case 5, while Lei et al. and Wang et al. methods have not demonstrated so good results. It is well known that implanted bearing faults have severe level in comparison to those naturally developed and this is major reason why Lei et al. and Wang et al. methods are successful in diagnosis of faults, presented in Cases 3 and 4.
- (3) In the proposed new improved Kurtogram, the selection of M value needs to be further investigated. Different M value will lead to different results. Recently, the fault diagnosis becomes a hot research topic and can save great cost for customers. Extracting degradation indicator, which can reflect the bearing state condition using proposed new improved Kurtogram automatically, will be researched in future. A good degradation indicator will be useful for the remaining useful life prediction [34].

4. Conclusions

This paper proposes a new CK value based Kurtogram, called a new improved Kurtogram that uses time synchronous

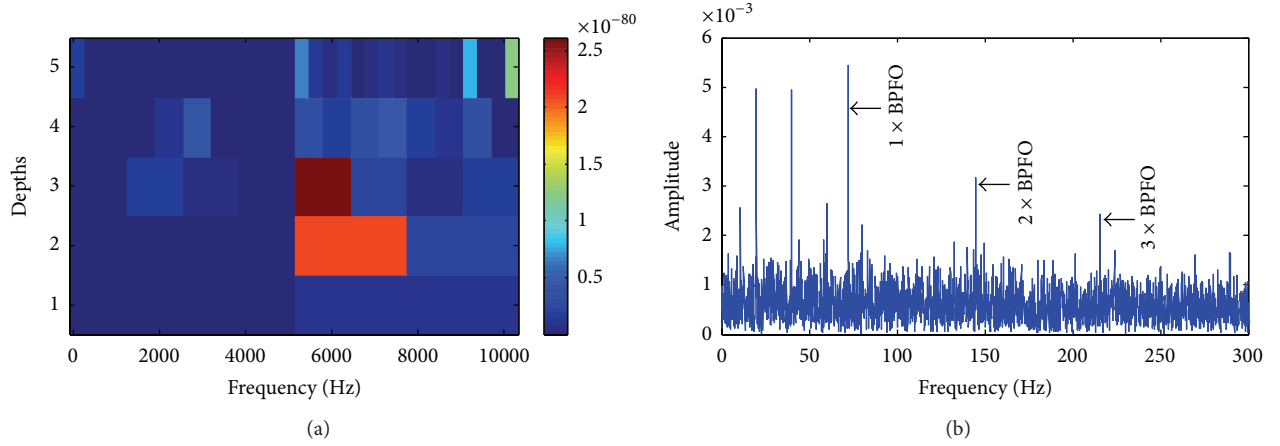


FIGURE 30: The results obtained by the proposed method for processing the outer race fault of 6205 bearing in gearbox. (a) The new improved Kurtogram and (b) power spectrum of the envelope of the signal extracted from node (3, 5) by WPD.

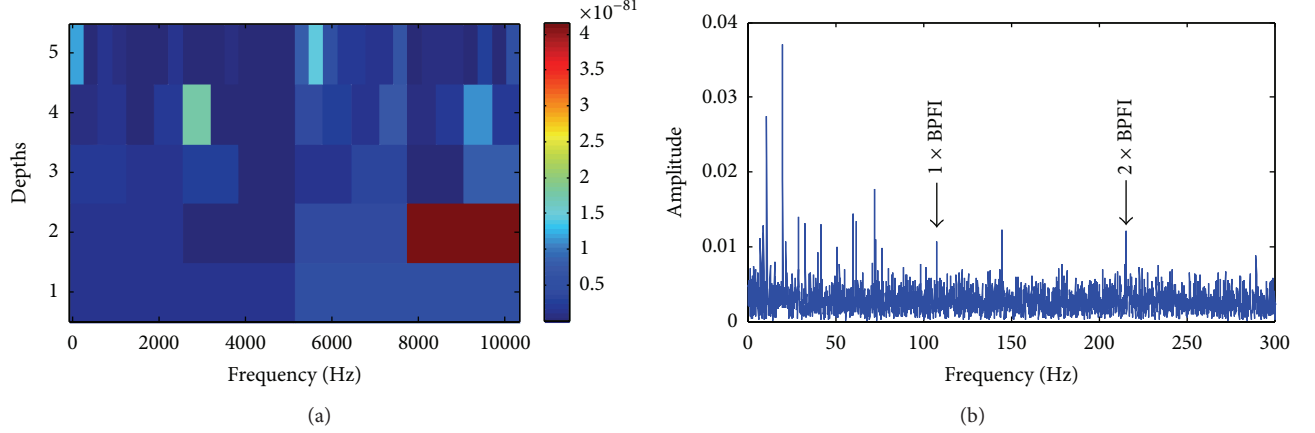


FIGURE 31: The results obtained by the proposed method for processing the inner race fault of 6205 bearing in gearbox. (a) The new improved Kurtogram and (b) power spectrum of the envelope of the signal extracted from node (2, 4) by WPD.

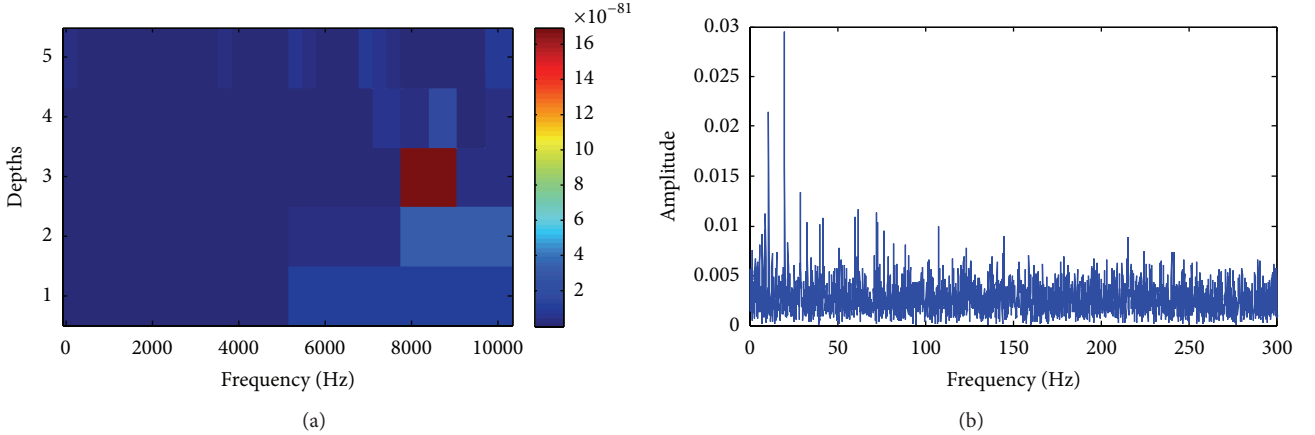


FIGURE 32: The results obtained by the proposed method for processing the ball fault of 6205 bearing in gearbox. (a) The new improved Kurtogram and (b) power spectrum of the envelope of the signal extracted from node (3, 7) by WPD.

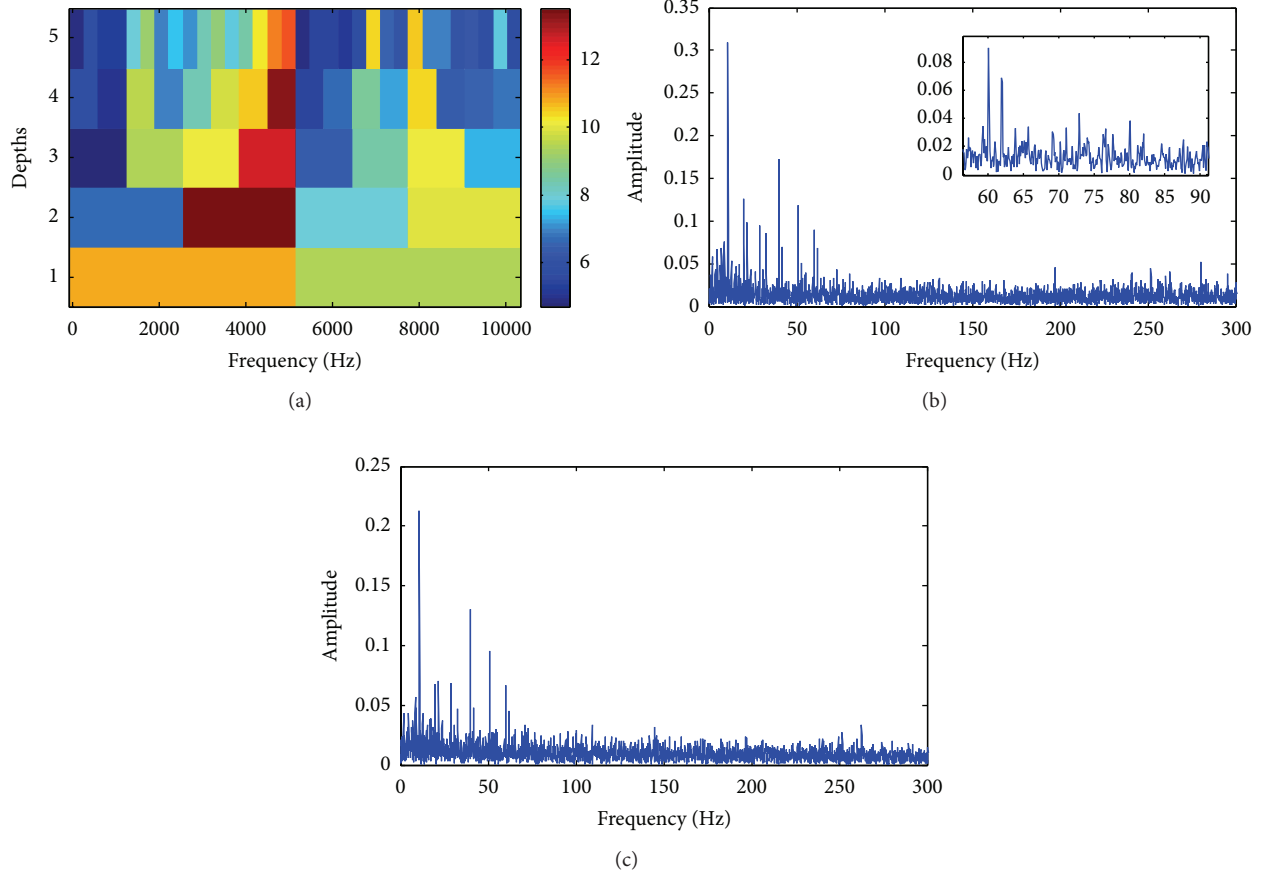


FIGURE 33: The results obtained by the improved Kurtogram proposed by Lei et al. for processing the 6205 bearing in gearbox. (a) The improved Kurtogram, (b) power spectrum of the envelope of the signal extracted from node (2, 2) by WPD, and (c) power spectrum of the envelope signal extracted from node (4, 8) by WPD.

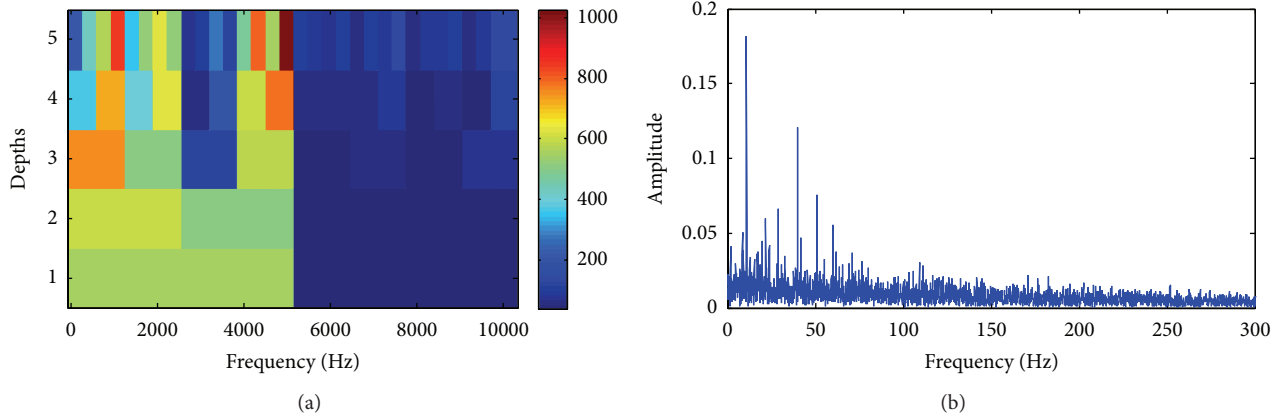


FIGURE 34: The results obtained by the enhanced Kurtogram proposed by Wang et al. for processing the 6205-bearing fault in gearbox. (a) The enhanced Kurtogram and (b) power spectrum of the envelope of the signal extracted from node (5, 16) by wavelet packet transform.

technique to separate the discrete frequency in first step using De-phase algorithm. Then, WPD was used to decompose and reconstruct the signal and after this step CK value was used as an indicator to select the optimal node which contains the impulse signal produced by bearing fault. Two

simulated bearing fault signals were used to demonstrate the method's effectiveness. New improved Kurtogram can detect the bearing fault even if the SNR is very low. Two implanted bearing fault data sets and one naturally developed bearing fault data set were used to further validate the

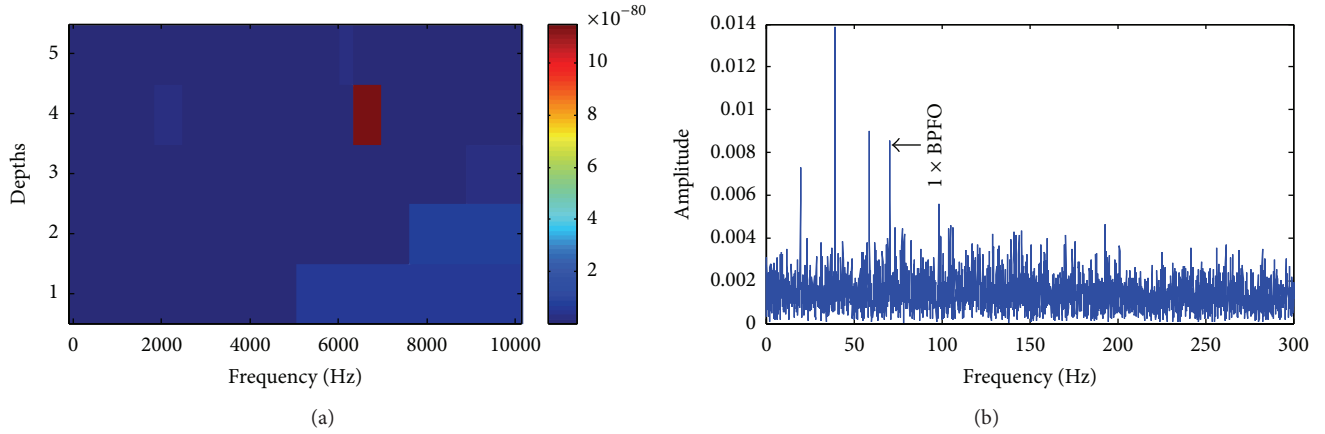


FIGURE 35: The results obtained by the proposed method for processing the outer race fault of 6205 bearing in gearbox under load 405 Nm. (a) The new improved Kurtogram and (b) power spectrum of the envelope of the signal extracted from node (4, 11) by WPD.

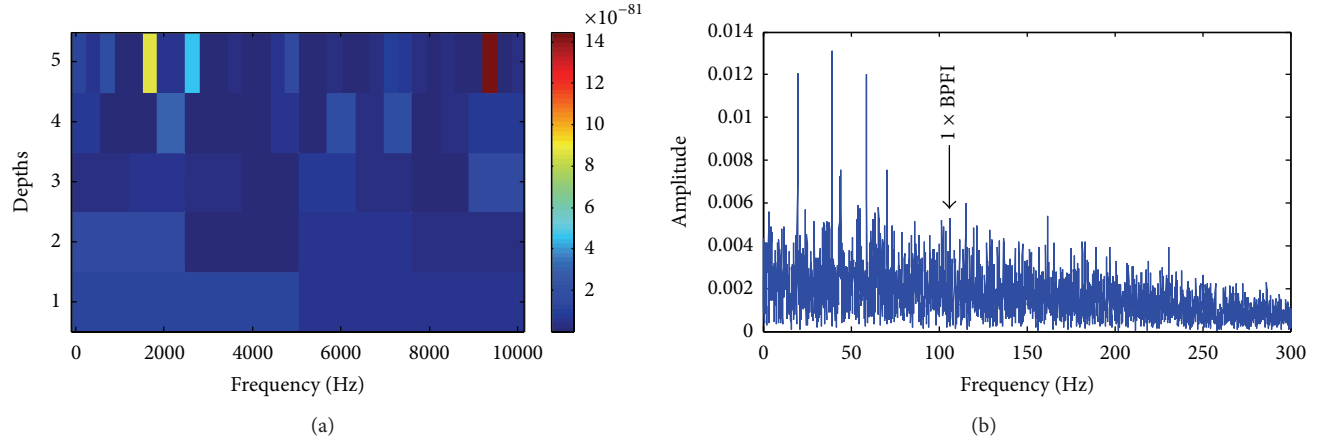


FIGURE 36: The results obtained by the proposed method for processing the inner race fault of 6205 bearing in gearbox under load 405 Nm. (a) The new improved Kurtogram and (b) power spectrum of the envelope of the signal extracted from node (5, 30) by WPD.

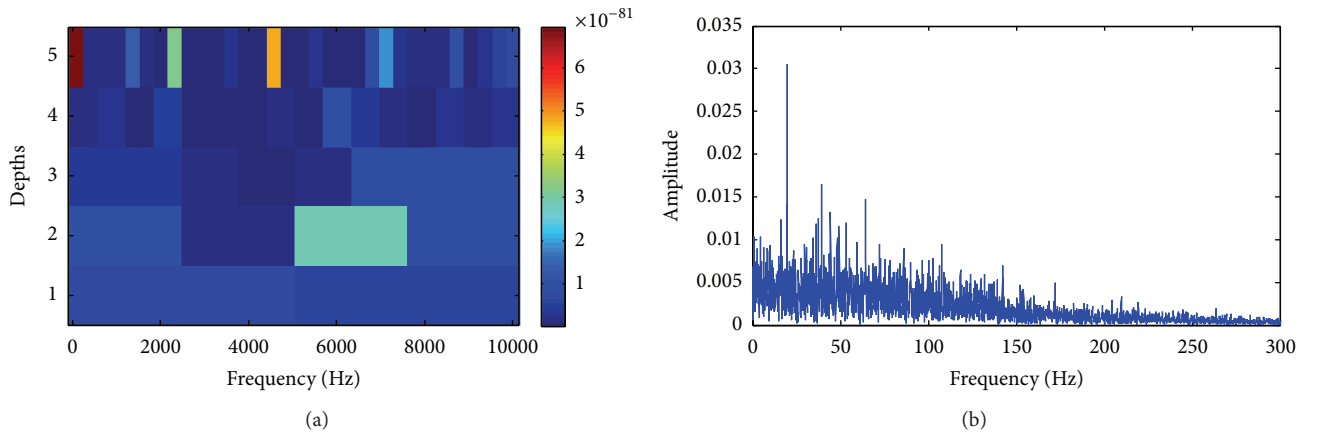


FIGURE 37: The results obtained by the proposed method for processing the ball fault of 6205 bearing in gearbox under load 405 Nm. (a) the new improved Kurtogram and (b) power spectrum of the envelope of the signal extracted from node (5, 1) by WPD.

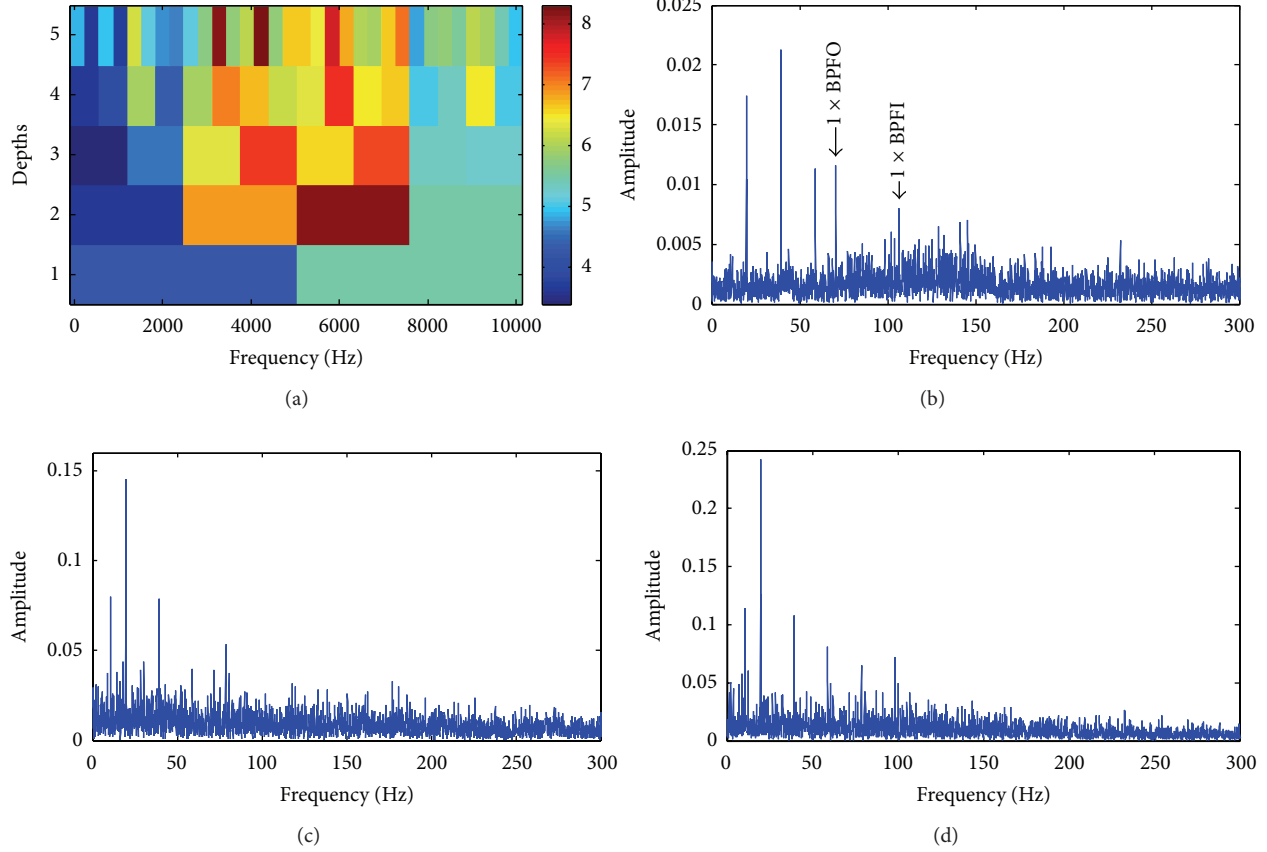


FIGURE 38: The results obtained by the improved Kurtogram proposed by Lei et al. for processing the 6205 bearing in gearbox under load 405 Nm. (a) the improved Kurtogram, (b) power spectrum of the envelope of the signal extracted from node (2,3) by WPD, (c) power spectrum of the envelope signal extracted from node (5,11) by WPD, (d) power spectrum of the envelope signal extracted from node (5,14) by WPD.

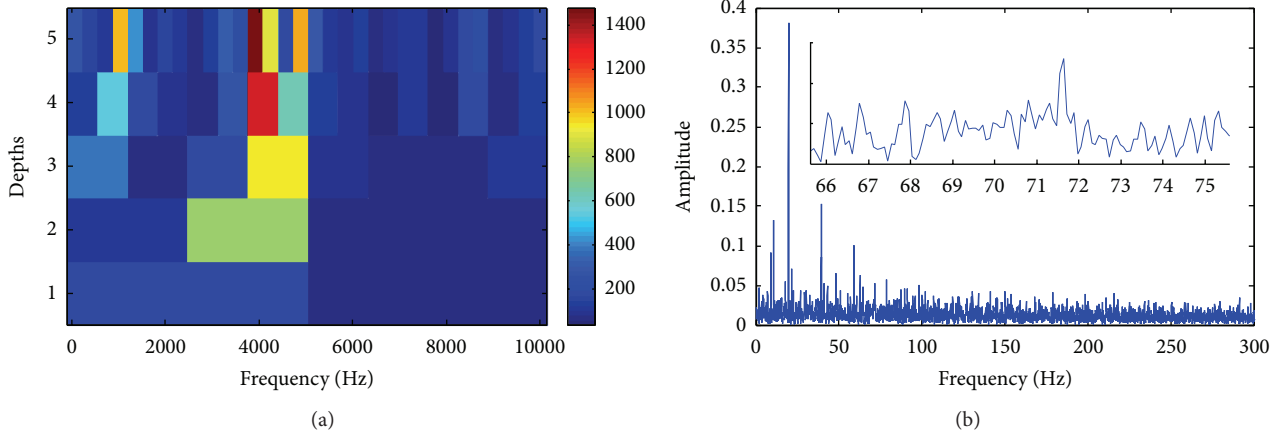


FIGURE 39: The results obtained by the enhanced Kurtogram proposed by Wang et al. for processing the 6205-bearing fault in gearbox under load 405 Nm. (a) The enhanced Kurtogram and (b) power spectrum of the envelope of the signal extracted from node (5,13) by WPD.

proposed method. Compared to the methods of Lei et al. and Wang et al., new improved Kurtogram can detect the bearing faults more precisely. However, the ball fault is not able to be detected using proposed method since this type of

fault is too weak compared to other bearing faults especially with presence of gear faults. Based on proposed method, extraction of degradation indicator will be researched in future.

Conflict of Interests

The authors declare that there is no conflict of interests regarding the publication of this paper.

Acknowledgments

This project was supported in part by the Natural Science Foundation of Hebei Province (E2015506012) and China Scholarship Council.

References

- [1] A. Lesmerises and D. Crowley, "Effect of different workscope strategies on wind turbine gearbox life cycle repair costs," *International Journal of Prognostics and Health Management*, vol. 4, article 017, 7 pages, 2013.
- [2] J. S. Lin and Q. Chen, "Fault diagnosis of rolling bearings based on multifractal detrended fluctuation analysis and Mahalanobis distance criterion," *Mechanical Systems and Signal Processing*, vol. 38, no. 2, pp. 515–533, 2013.
- [3] X. Y. Zhang and J. Z. Zhou, "Multi-fault diagnosis for rolling element bearings based on ensemble empirical mode decomposition and optimized support vector machines," *Mechanical Systems and Signal Processing*, vol. 41, no. 1-2, pp. 127–140, 2013.
- [4] X. H. Zhang, L. Xiao, and J. S. Kang, "Application of an improved Levenberg-Marquardt back propagation neural network to gear fault level identification," *Journal of Vibroengineering*, vol. 16, pp. 855–868, 2014.
- [5] R. B. Randall and J. Antoni, "Rolling element bearing diagnostics—a tutorial," *Mechanical Systems and Signal Processing*, vol. 25, no. 2, pp. 485–520, 2011.
- [6] N. Sawalhi, R. B. Randall, and H. Endo, "The enhancement of fault detection and diagnosis in rolling element bearings using minimum entropy deconvolution combined with spectral kurtosis," *Mechanical Systems and Signal Processing*, vol. 21, no. 6, pp. 2616–2633, 2007.
- [7] T. Barszcz and N. Sawalhi, "Wind turbines' rolling element bearings fault detection enhancement using minimum entropy deconvolution," *Diagnostyka-Diagnostics and Structural Health Monitoring*, no. 3, pp. 53–59, 2011.
- [8] G. L. McDonald, Q. Zhao, and M. J. Zuo, "Maximum correlated Kurtosis deconvolution and application on gear tooth chip fault detection," *Mechanical Systems and Signal Processing*, vol. 33, pp. 237–255, 2012.
- [9] M. Karimi, *Rolling element bearing fault diagnostics using the blind deconvolution technique [Ph.D. thesis]*, School of Engineering Systems, Faculty of Built Environmental Engineering, Queensland University of Technology, 2006.
- [10] A. S. Raj and N. Murali, "A novel application of Lucy-Richardson deconvolution: bearing fault diagnosis," *Journal of Vibration and Control*, vol. 21, no. 6, pp. 1055–1067, 2015.
- [11] T. Barszcz and A. Jabłoński, "A novel method for the optimal band selection for vibration signal demodulation and comparison with the Kurtogram," *Mechanical Systems and Signal Processing*, vol. 25, no. 1, pp. 431–451, 2011.
- [12] Y. G. Lei, J. Lin, Z. J. He, and Y. Y. Zi, "Application of an improved kurtogram method for fault diagnosis of rolling element bearings," *Mechanical Systems and Signal Processing*, vol. 25, no. 5, pp. 1738–1749, 2011.
- [13] D. Wang, P. W. Tse, and K. L. Tsui, "An enhanced Kurtogram method for fault diagnosis of rolling element bearings," *Mechanical Systems and Signal Processing*, vol. 35, no. 1-2, pp. 176–199, 2013.
- [14] B. Q. Chen, Z. S. Zhang, Y. Y. Zi, Z. J. He, and C. Sun, "Detecting of transient vibration signatures using an improved fast spatial-spectral ensemble kurtosis kurtogram and its applications to mechanical signature analysis of short duration data from rotating machinery," *Mechanical Systems and Signal Processing*, vol. 40, no. 1, pp. 1–37, 2013.
- [15] J. Antoni, "The spectral kurtosis: a useful tool for characterising non-stationary signals," *Mechanical Systems and Signal Processing*, vol. 20, no. 2, pp. 282–307, 2006.
- [16] J. Antoni, "Fast computation of the kurtogram for the detection of transient faults," *Mechanical Systems and Signal Processing*, vol. 21, no. 1, pp. 108–124, 2007.
- [17] Y. Wang and M. Liang, "Identification of multiple transient faults based on the adaptive spectral kurtosis method," *Journal of Sound and Vibration*, vol. 331, no. 2, pp. 470–486, 2012.
- [18] Y. X. Wang and M. Liang, "An adaptive SK technique and its application for fault detection of rolling element bearings," *Mechanical Systems and Signal Processing*, vol. 25, no. 5, pp. 1750–1764, 2011.
- [19] P. W. Tse and D. Wang, "The design of a new sparsogram for fast bearing fault diagnosis: part 1 of the two related manuscripts that have a joint title as 'Two automatic vibration-based fault diagnostic methods using the novel sparsity measurement-Parts 1 and 2,'" *Mechanical Systems and Signal Processing*, vol. 40, no. 2, pp. 499–519, 2013.
- [20] P. W. Tse and D. Wang, "The automatic selection of an optimal wavelet filter and its enhancement by the new sparsogram for bearing fault detection. Part 2 of the two related manuscripts that have a joint title as 'two automatic vibration-based fault diagnostic methods using the novel sparsity measurement. Parts 1 and 2,'" *Mechanical Systems and Signal Processing*, vol. 40, no. 2, pp. 520–544, 2013.
- [21] H. Y. Liu, W. G. Huang, S. B. Wang, and Z. K. Zhu, "Adaptive spectral kurtosis filtering based on Morlet wavelet and its application for signal transients detection," *Signal Processing*, vol. 96, pp. 118–124, 2014.
- [22] N. Bouguerriou, M. Haritopoulos, C. Capdessus, and L. Allam, "Novel cyclostationarity-based blind source separation algorithm using second order statistical properties: theory and application to the bearing defect diagnosis," *Mechanical Systems and Signal Processing*, vol. 19, no. 6, pp. 1260–1281, 2005.
- [23] P. W. Tse, S. Gontarz, and X. J. Wang, "Enhanced eigenvector algorithm for recovering multiple sources of vibration signals in machine fault diagnosis," *Mechanical Systems and Signal Processing*, vol. 21, no. 7, pp. 2794–2813, 2007.
- [24] D. Wang and P. W. Tse, "A new blind fault component separation algorithm for a single-channel mechanical signal mixture," *Journal of Sound and Vibration*, vol. 331, pp. 4956–4970, 2012.
- [25] Z. X. Li, X. P. Yan, Z. Tian, C. Q. Yuan, Z. X. Peng, and L. Li, "Blind vibration component separation and nonlinear feature extraction applied to the nonstationary vibration signals for the gearbox multi-fault diagnosis," *Measurement*, vol. 46, no. 1, pp. 259–271, 2013.
- [26] H. Zhang, G. Wang, P. Cai, Z. Wu, and S. Ding, "A fast blind source separation algorithm based on the temporal structure of signals," *Neurocomputing*, vol. 139, pp. 261–271, 2014.

- [27] A. Keziou, H. Fenniri, A. Ghazdali, and E. Moreau, "New blind source separation method of independent/dependent sources," *Signal Processing*, vol. 104, pp. 319–324, 2014.
- [28] W. L. Hwang and J. Ho, "Null space component analysis for noisy blind source separation," *Signal Processing*, vol. 109, pp. 301–316, 2015.
- [29] R. Klein, E. Rudyk, E. Masad, and M. Issacharoff, "Emphasizing bearing tones for prognostics," *The International Journal of Condition Monitoring*, vol. 1, pp. 73–78, 2011.
- [30] Fault Data Sets, 2013, <http://www.mfpt.org/>.
- [31] R. Li, P. Sopon, and D. He, "Fault features extraction for bearing prognostics," *Journal of Intelligent Manufacturing*, vol. 23, no. 2, pp. 313–321, 2012.
- [32] H. Li, Y. P. Zhang, and H. Q. Zheng, "Application of Hermitian wavelet to crack fault detection in gearbox," *Mechanical Systems and Signal Processing*, vol. 25, no. 4, pp. 1353–1363, 2011.
- [33] X. Zhang, J. Kang, E. Bechhoefer, and J. Zhao, "A new feature extraction method for gear fault diagnosis and prognosis," *Eksplotacja i Niezawodnosc-Maintenance and Reliability*, vol. 16, no. 2, pp. 295–300, 2014.
- [34] X. H. Zhang, J. S. Kang, and T. Jin, "Degradation modeling and maintenance decisions based on Bayesian belief networks," *IEEE Transactions on Reliability*, vol. 63, no. 2, pp. 620–633, 2014.

